The Plant Cell, Vol. 30: 375–396, February 2018, www.plantcell.org © 2018 ASPB.

OPAQUE11 Is a Central Hub of the Regulatory Network for Maize Endosperm Development and Nutrient Metabolism[OPEN]

Fan Feng,[a] Weiwei Qi,[a] Yuanda Lv,[b] Shumei Yan,[a] Liming Xu,[a] Wenyao Yang,[a] Yue Yuan,[a] Yihan Chen,[a] Han Zhao,[b] and Rentao Song[a,c,1]

[a] Shanghai Key Laboratory of Bio-Energy Crops, Plant Science Center, School of Life Sciences, Shanghai University, Shanghai 200444, China

[b] Institute of Biotechnology, Jiangsu Provincial Key Laboratory of Agrobiology, Jiangsu Academy of Agricultural Sciences, Nanjing 210014, China

[c] National Maize Improvement Center of China, China Agricultural University, Beijing 100193, China

ORCID IDs: 0000-0001-6877-000X (H.Z.); 0000-0003-1810-9875 (R.S.)

Maize (*Zea mays*) endosperm is a primary tissue for nutrient storage and is highly differentiated during development. However, the regulatory networks of endosperm development and nutrient metabolism remain largely unknown. Maize *opaque11* (*o11*) is a classic seed mutant with a small and opaque endosperm showing decreased starch and protein accumulation. We cloned *O11* and found that it encodes an endosperm-specific bHLH transcription factor (TF). Loss of function of O11 significantly affected transcription of carbohydrate/amino acid metabolism and stress response genes. Genome-wide binding site analysis revealed 9885 O11 binding sites distributed over 6033 genes. Using chromatin immunoprecipitation sequencing (ChIP-seq) coupled with RNA sequencing (RNA-seq) assays, we identified 259 O11-modulated target genes. O11 was found to directly regulate key TFs in endosperm development (NKD2 and ZmDOF3) and nutrient metabolism (O2 and PBF). Moreover, O11 directly regulates cyPPDKs and multiple carbohydrate metabolic enzymes. O11 is an activator of *ZmYoda*, suggesting its regulatory function through the MAPK pathway in endosperm development. Many stress-response genes are also direct targets of O11. In addition, 11 O11-interacting proteins were identified, including *ZmIce1*, which coregulates stress response targets and *ZmYoda* with O11. Therefore, this study reveals an endosperm regulatory network centered around O11, which coordinates endosperm development, metabolism and stress responses.

INTRODUCTION

Maize (*Zea mays*) is one of the most important crops in the world and a model system for genetic and molecular biology studies. Maize endosperm, as a primary storage tissue, is a product of double fertilization, which produces a diploid embryo as well as the triploid endosperm (Russell, 1992; Kiesselbach, 1949). The fully developed maize endosperm includes four highly differentiated cell types: the aleurone (AL), the starchy endosperm (SE), the basal endosperm transfer layer (BETL), and the embryo-surrounding region (ESR) (Olsen, 2001; Becraft and Gutierrez-Marcos, 2012; Leroux et al., 2014). The AL is a single peripheral layer of cells that produces hydrolytic enzymes to mobilize storage in the SE when the seed begins germination. The SE stores starch and storage protein for the preparation of seed germination. The BETL is a dendritic transfer cell layer that transports nutrients from the maternal tissue to the endosperm. The ESR is defined by a group of cells that share ESR gene family expression and is believed to act as a physical barrier and a messenger between the endosperm and the embryo (Opsahl-Ferstad et al., 1997).

Maize endosperm development is controlled by sophisticated regulatory networks, with transcription factors (TFs) playing important roles. Genetic and molecular evidence has revealed a number of TFs that have key functions in endosperm development. Naked endosperm 1 (NKD1) and NKD2 are duplicate indeterminate domain TFs that regulate endosperm cell patterning and differentiation (Yi et al., 2015). Gontarek et al. (2016) demonstrated that NKDs modulate a series of biological processes in endosperm development, including gene expression, epigenetic functions, cell growth and division, hormone signaling, and resource reserve deposition and are direct upstream regulators of *Opaque2* (*O2*) and *Viviparous1* (*VP1*). VP1 functions as an activator of abscisic acid-induced genes for seed maturation and is also a repressor of germination-specific genes (McCarty et al., 1991; Hoecker et al., 1995). Another maize endosperm-specific DOF TF, ZmDOF3, is reportedly a direct activator of NKDs and a key regulator in starch accumulation and endosperm development (Qi et al., 2017). Thus, the identification and functional analysis of key TFs are important for understanding the mechanisms of endosperm development.

Starch and storage proteins are the primary nutrient components of maize endosperm, with starch accounting for ~75% of the dry weight of maize kernels. Starch is synthesized in specialized amyloplasts via a process that involves the activity of four major enzymes: granule-bound starch synthase, starch synthases, starch-branching enzymes, and debranching enzymes (James et al., 2003). Protein accounts for ~8% of the maize kernel dry weight, with ~60% of this protein being prolamins, also named zeins. Cytoplasmic pyruvate orthophosphate dikinase 1 and

[1] Address correspondence to rentaosong@cau.edu.cn.
The author responsible for distribution of materials integral to the findings presented in this article in accordance with the policy described in the Instructions for Authors (www.plantcell.org) is: Rentao Song (rentaosong@cau.edu.cn).

[OPEN]Articles can be viewed without a subscription.
www.plantcell.org/cgi/doi/10.1105/tpc.17.00616

2 (cyPPDKs) are considered key molecular switches in the balance between starch and protein accumulation (Sheen, 1991; Prioul et al., 2008; Manicacci et al., 2009), and as an endosperm-specific bZIP TF, O2 positively regulates the *cyPpdk* genes and nearly all zein genes (Schmidt et al., 1987; Li et al., 2015). Loss of function of O2 results in a drastically decreased zein content and smaller protein bodies (PBs). Prolamin-box binding factor (PBF), another endosperm-specific DOF TF, directly interacts with O2 to regulate zein synthesis (Vicente-Carbajosa et al., 1997; Wu and Messing, 2012) and *cyPpdk* genes (Zhang et al., 2016). Therefore, elaborate regulatory networks involving TFs ensure efficient nutrient storage in the maize endosperm, though only a few have been studied to date.

In this study, we report the identification of a classic maize mutant, *opaque11* (*o11*) (Nelson, 1981). *o11* exhibits a reduced endosperm and unbalanced starch and protein accumulation. Through positional cloning, we found that *O11* encodes a cereal endosperm-specific basic helix-loop-helix (bHLH) TF. Genome-wide identification of its binding targets revealed a regulatory network centered around O11, which coordinates cell development, storage nutrient metabolism, and stress responses in the maize endosperm.

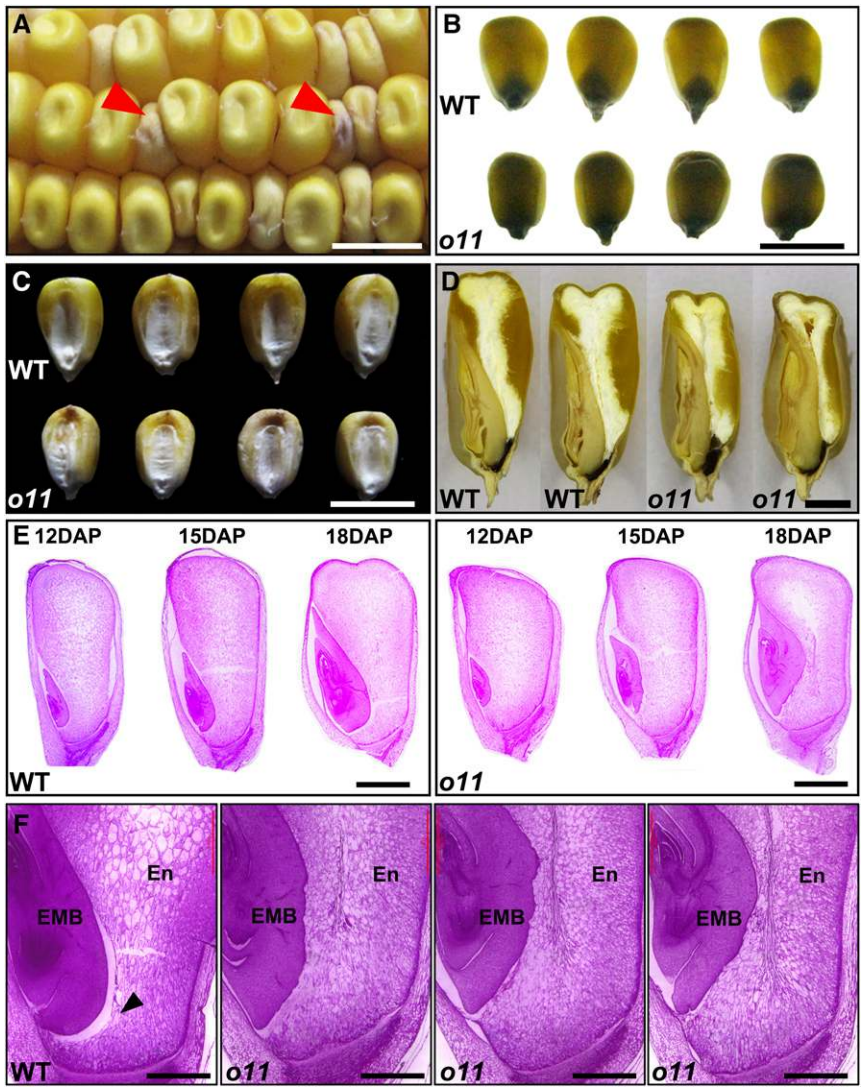

Figure 1. Phenotypic Features of *o11*.

(A) An F2 ear of *o11* X W22. Red arrowheads indicate typical *o11* kernels. Bar = 1 cm.
(B) Wild-type (WT) and *o11* mature kernels viewed on a light box. Bar = 1 cm.
(C) Wild-type and *o11* mature kernels viewed under natural light. Bar = 1 cm.
(D) Longitudinal sections of wild-type and *o11* mature kernels. Bar = 2 mm.
(E) Longitudinal sections of developing wild type and *o11* kernels at 12, 15, and 18 DAP. Bars = 2 mm.
(F) High-magnification longitudinal sections of developing wild type and *o11* kernels at 18 DAP. The first image is a wild-type kernel, and the other three are *o11* kernels. The arrowhead in the wild type indicates the interface between the embryo and the endosperm. EMB, embryo; En, endosperm. Bars = 1 mm.

RESULTS

o11 Has a Reduced and Opaque Endosperm with Developmental Defects

The *o11* mutant obtained from the Maize Genetics Cooperation Stock Center was crossed into the W22 genetic background. On the F2 ears, *o11* kernels exhibited 1:3 segregation to the wild-type kernels, indicating that *o11* is a single recessive mutant (Supplemental Figure 1A). Mature *o11* kernels had less vitreous endosperm and were significantly smaller compared with wild-type kernels (Figures 1A to 1C). The 100-kernel weight of *o11* mutants was 32.3% less than that of the wild type (Supplemental Figure 1B). In the *o11* mutant, the endosperm was more severely affected than the embryo by the mutation of *O11* (Figure 1D; Supplemental Figures 1C and 1D). The SE region was greatly reduced, and its central region was empty (Figures 1D and 1E). The morphology of the *o11* embryo was also affected in that the middle region of the *o11* embryo's scutellum was thicker and the bottom region was narrower compared with the wild type (Figure 1E). Furthermore, we observed morphological changes around the ESR: Although an apparent interspace between the embryo and the ESR region was found in wild-type kernels, little space was observed in the same region in *o11* mutant kernels (Figure 1F; Supplemental Figure 2). Wild-type kernels also exhibited clear and smooth boundaries at the interface between the scutellum and the surrounding endosperm, whereas *o11* showed unclear and zigzagged boundaries (Figure 1F; Supplemental Figure 2). The germination rate and reproductive growth of homozygous *o11* mutants were not affected, despite a mild growth delay in early seedlings.

o11 Has Less Starch and Protein Accumulation

Cytological observation of both the developing (Figure 2A) and mature (Figure 2B) endosperm indicated that the starch granules in *o11* endosperm were smaller than those of the wild type. PBs were also smaller in *o11* than in the wild type (Figure 2C). Biochemical analysis indicated that compared with the wild type, the total starch, protein and lipid contents of *o11* endosperm per kernel were all decreased (~34.2% less for total starch, ~25.0% less for total protein, and ~15.3% less for total lipid) (Figures 2D to 2F). When these storage nutrients were measured according to equal biomass, we found the starch content of the *o11* endosperm to still be decreased per weight (Supplemental Figure 3A), but the total protein and lipid contents were increased (Supplemental Figures 3B and 3C). The C/N ratio of the *o11* endosperm was also decreased compared with that of the wild type (Figure 2G). Moreover, the *o11* endosperm showed a higher total amino acid content for most amino acids (Supplemental Figure 4A), and the free proline content of *o11* was four times higher than that of the wild type (Supplemental Figure 4B).

Map-Based Cloning and Identification of O11

Using 9900 mutant kernels from a BC1F1 population, the *O11* gene was genetically mapped to a 900-kb genomic interval on chromosome 2 (Figure 3A). This interval contained 14 predicted genes. RNA-seq analysis of wild-type and *o11* kernels at 15 d after

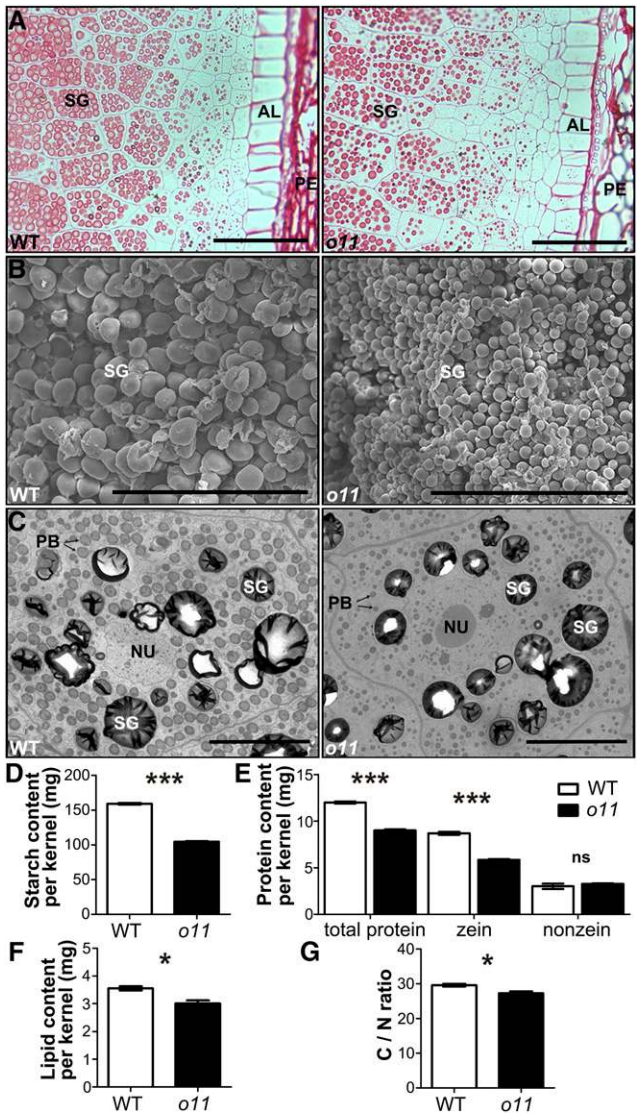

Figure 2. Cytological and Biochemical Analysis of Wild-Type and *o11* Endosperm.

(A) Resin sections of developing endosperm of wild type and *o11* kernel at 18 DAP. Bars = 100 μm.

(B) Scanning electron microscopy of the central regions of the mature endosperm of the wild type and *o11* kernel. Bars = 100 μm.

(C) Transmission electron microscopy of 18-DAP endosperm of the wild type and *o11* at the fourth cell layer from the AL. Bars = 10 μm.

AL, aleurone; NU, nucleus; PB, protein body; PE, pericarp; SG, starch granule.

(D) to **(F)** Comparison of starch **(D)**, protein (total protein, zein, and nonzein) **(E)**, and lipid **(F)** contents per kernel of the mature wild type and *o11* endosperm.

(G) The carbon/nitrogen (C/N) ratio in mature wild-type and *o11* endosperm. Error bars indicate ±SE ($n = 3$). *$P < 0.05$ and ***$P < 0.001$; ns, not significant; Student's *t* test.

pollination (DAP) revealed only a few single-nucleotide polymorphisms in most of the predicted genes. However, a 3864-bp retrotransposon insertion was found at the 3′ end of the 2nd exon of *GRMZM2G147685* (Figures 3B to 3D).

A functional complementation test was performed by transforming an 8464-bp *GRMZM2G147685* genomic fragment amplified from the wild-type genome (containing 2311 bp upstream of the start codon and 1019 bp downstream of the stop codon) into maize (pApB, Hi-II hybrid). Based on genotyping analysis, *o11/o11* kernels carrying the transgenic *GRMZM2G147685* genomic fragment were functionally complemented, with the *o11* mutant pheotype rescued (Figures 4A to 4C). We also produced *GRMZM2G147685* knockout mutant alleles (five alleles, *o11-cas9-1* to *o11-cas9-5*; Supplemental Figure 5A) using the CRISPR-Cas9 system (Qi et al., 2016a) and performed allelism tests by crossing two independent knockout alleles (*o11-cas9-1* and *o11-cas9-2*) to *o11-ref* (Figures 4D to 4G; Supplemental Figure 5B). In allelism tests, kernels displayed a mutant phenotype similar to that of *o11*, indicating that *o11-cas9* alleles cannot complement *o11-ref* (Figures 4E and 4F; Supplemental Figure 5B). All these results indicate that *GRMZM2G147685* is *O11*.

Using an antibody raised against the protein encoded by *GRMZM2G147685*, we detected a single specific band with a molecular mass of ~90 kD in wild-type kernels, whereas this protein was not detectable in *o11-ref* or *o11-cas9-1* kernels (Figure 3E). Therefore, the loss of O11 function is caused by a retrotransposon

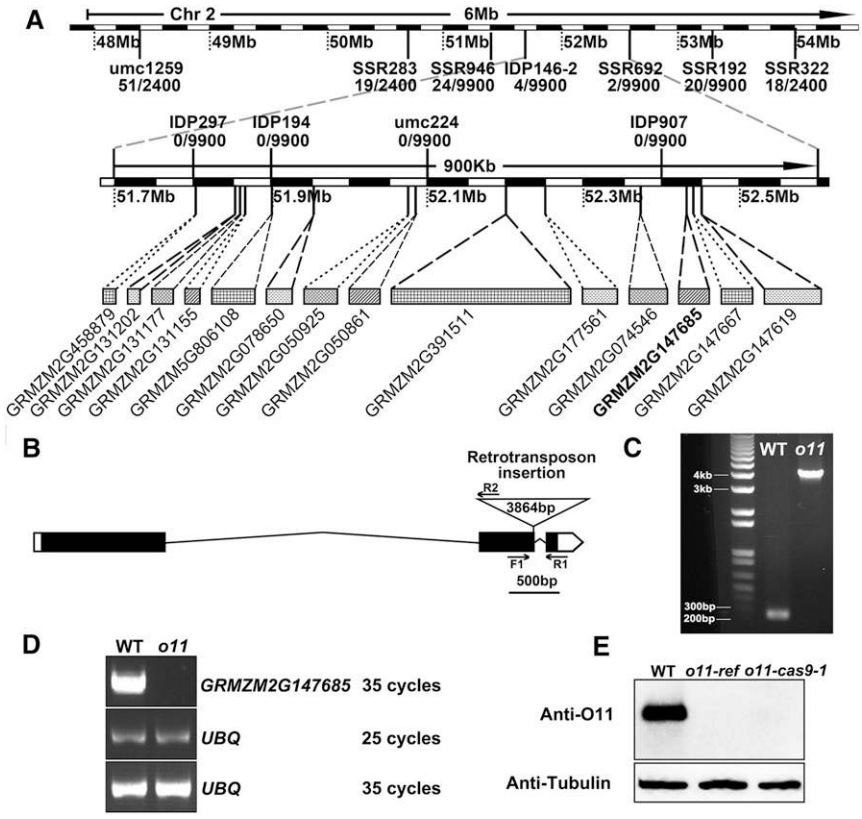

Figure 3. Map-Based Cloning and Identification of O11.

(A) Fine-mapping of *o11*. The *o11-ref* mutant was crossed into the W22 inbred line and then backcrossed with *o11-ref* to generate a BC1F1 mapping population. Approximately 9900 mutant kernels from the BC1F1 population were characterized, and the *o11* gene was mapped to between the molecular markers IDP146-2 and SSR692. The number under each molecular marker indicates the number of recombinants versus the tested population size between *o11* and the molecular marker. The physical positions in Mb of chromosome 2 from the short-arm telomere are indicated next to the dotted vertical lines (beneath the zebra bars). Predicted candidate genes with their gene number are indicated as horizontal bars beneath the lower zebra bar.

(B) A diagram showing the *GRMZM2G147685* gene structure and the insertion site of the retrotransposon. Black boxes represent exons, and lines represent introns. The open box and open arrow represent the 5′ and 3′ untranslated regions, respectively. The triangle represents the retrotransposon, which is inserted into the 2nd exon. The number inside the triangle indicates the size of the retrotransposon in bp. Arrows indicate the primers used for amplification of the retrotransposon insertion junction in **(C)** (F1 and R1) and Figure 4G (F1 and R2).

(C) Amplification of the retrotransposon from homozygous wild-type and *o11* genomic DNA using the F1 and R1 primers indicated in Figure 2B.

(D) Amplification of the *GRMZM2G147685* coding sequence from 18-DAP endosperm cDNA. The *ubiquitin* (*UBQ*) gene was used as a control amplified using 25 or 35 cycles.

(E) Immunoblot analysis with an anti-O11 antibody. Approximately 20 μg total protein extract from 18-DAP wild type, *o11-ref*, or *o11-cas9-1* whole kernels was used. Antitubulin was employed as a sample loading control.

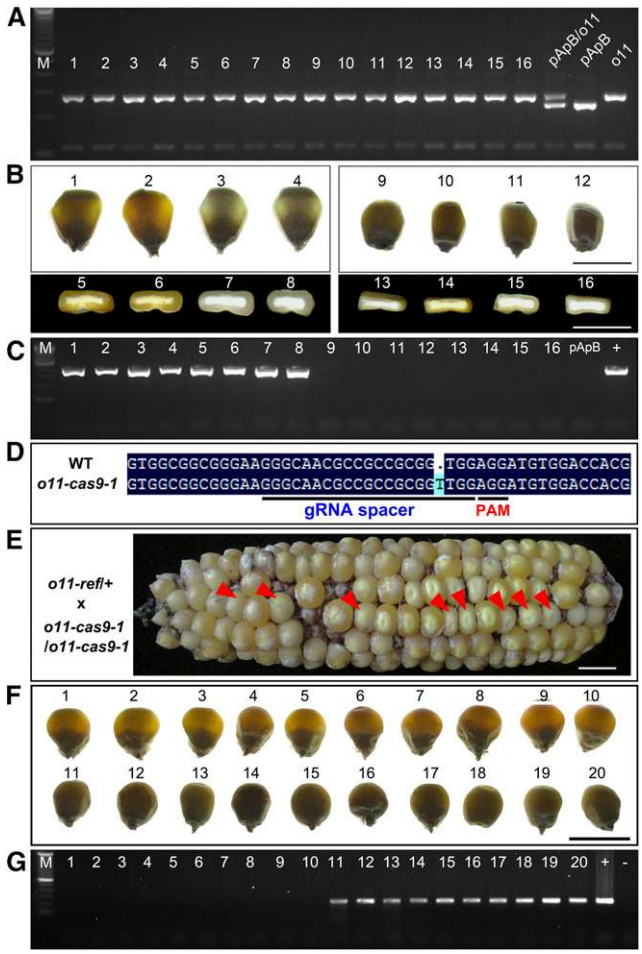

Figure 4. Functional Complementation Test and Allelism Test of *o11*.

(A) to **(C)** Functional complementation test of *o11*. Genomic DNA (8464 bp) containing the entire coding region of *GRMZM2G147685*, a 2311-bp upstream sequence, and a 1019-bp downstream sequence was transformed into the Hi-II hybrid pApB. Transgenic lines (T0) were crossed to the homozygous mutant (*o11*/*o11*) and then self-pollinated (T2 lines) to obtain functionally complemented kernels. Sixteen representative kernels containing homozygous *o11* alleles were identified using molecular marker F/R6, as F/R6 is tightly linked to the *o11* locus, and using homozygous *o11* (*o11*), pApB, and their F1 (pApB/*o11*) as controls **(A)**. Of these, eight kernels (1–8) showed the wild-type phenotype, and eight kernels (9–16) showed the small and opaque mutant phenotype. Bar = 1 cm in **(B)**. Primers for the *Bar* gene were used to identify whether these kernels contain the *GRMZM2G147685* transgene **(C)**. Kernels showing the wild-type phenotype were all transgene positive, whereas those showing the mutant phenotype were all transgene negative. +, *GRMZM2G147685* transgene construct as a positive control; pApB, pApB genomic DNA as a negative control.

(D) to **(G)** Allelism test between heterozygous *o11-ref* and homozygous *o11-cas9-1*.

(D) Diagram of the editing site in *o11-cas9-1*. *o11-cas9-1* contains a "T" insertion in the first exon of *GRMZM2G147685*. gRNA, guide RNA; PAM, protospacer adjacent motif.

(E) Allelism test of ear produced from a cross between heterozygous *o11-ref* (*o11-ref*/+) and homozygous *o11-cas9-1* (*o11-cas9-1*/*o11-cas9-1*). Red arrowheads indicate some mutant-phenotype kernels. Bar = 1 cm.

(F) Randomly selected kernels from Figure 4E (1–10 for wild type kernels; 11–20 for mutant kernels with the small and opaque phenotype) were viewed on a light box. Bar = 1 cm.

(G) Genotyping of the wild-type kernels (1–10) and mutant kernels (11–20) in Figure 4F using primers F1 and R2 (see Figure 3B) to identify the *o11-ref* allele. +, *o11-ref* genomic DNA as a positive control; −, water as a negative control.

insertion in the *GRMZM2G147685* coding region, which results in the absence of the O11 protein.

O11 Encodes a bHLH TF Specifically Expressed in the Endosperm

O11 is predicted to be a bHLH protein without other known conserved domains; the full-length protein contains 624 amino acids, with the bHLH domain from residues 379 to 430. Phylogenetic analysis showed that O11 homologous proteins could be grouped into two major clades represented by monocotyledonous and dicotyledonous species, respectively. O11 grouped into the monocotyledon clade, whereas ZHOUPI (AtZOU) from *Arabidopsis thaliana* (Yang et al., 2008) was in the dicotyledon clade (Figure 5A; Supplemental Data Set 1). Notably, O11 contained an extra 300 amino acids at the N terminus, which was found only in *Sorghum bicolor* and *Setaria italica* (Supplemental Figure 6).

O11 transcript accumulation was observed only in kernels, with a peak at 9 DAP (Figure 5B). At the protein level, O11 was detectable only in the endosperm (Figure 5C). O11 was first detectable at 9 DAP, peaking at 18 DAP and decreasing thereafter (Figure 5C). Immunofluorescence assays with *o11* mutant kernels as the negative control indicated that O11 was preferentially located in the nuclei of SE and ESR cells (Figure 6A). The subcellular localization of $35S_{pro}$:O11-YFP expressed in onion epidermal cells was mainly in the nucleus, with some localization in the cytoplasm (Figure 6B). Fractionation analysis of nuclear and cytoplasmic proteins of developing maize kernels (15 DAP) showed O11 to accumulate both in the nucleus and the cytoplasm (Figure 6C). A yeast transactivation assay was performed to investigate whether O11 possesses transcriptional activity, and weak transactivation capacity was observed (Figure 6D).

o11 Affects Transcription of Cellular Carbohydrate, Amino Acid Metabolism, and Stress Response Genes

To understand the molecular basis of the phenotypic defects of the *o11* mutant, significantly differentially expressed genes (DEGs) were identified from RNA-seq data generated by three independent biological replicates from pooled *o11* and wild-type kernels at 15 DAP. According to these RNA-seq data, mutation of O11 significantly alters the expression of 1031 genes ($P < 0.05$, fold change greater than 1.5), including 337 downregulated and 694 upregulated genes (Supplemental Data Set 2).

Among these DEGs, 575 genes were functionally annotated and classified using the Gene Ontology (GO) database (http://bioinfo.cau.edu.cn/agriGO/) (Figure 7A; Supplemental Data Set 3). Loss of function of O11 significantly affected cellular carbohydrate

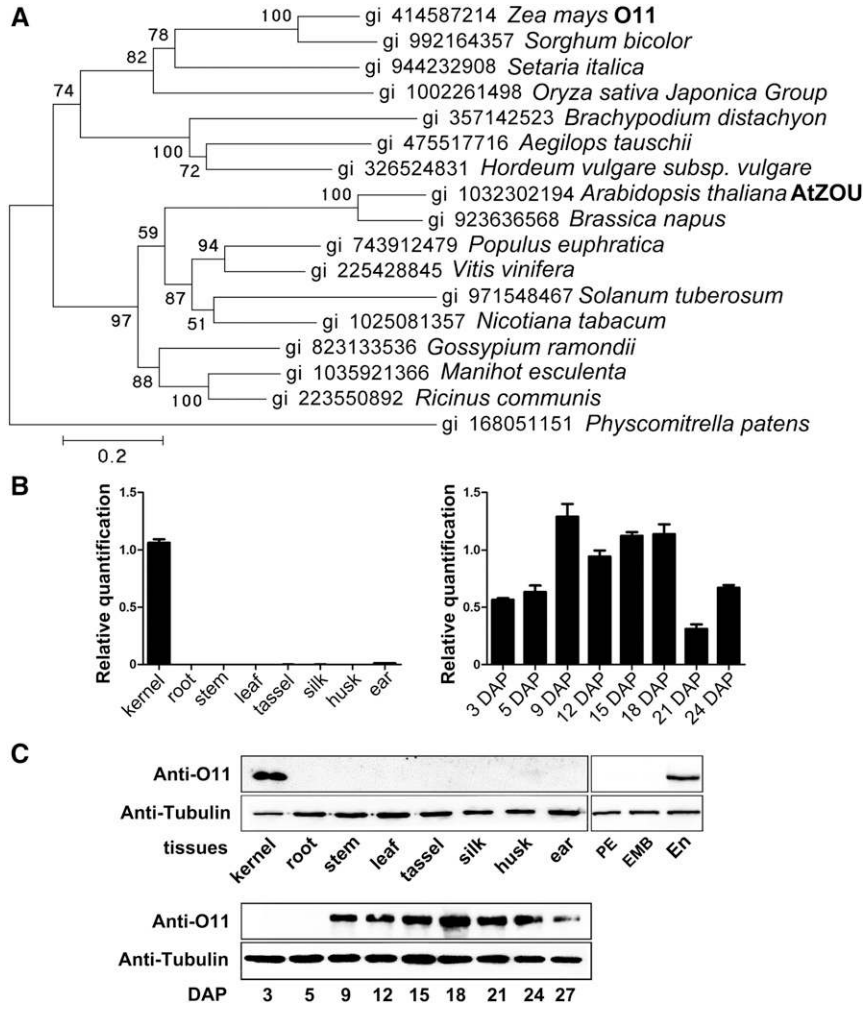

Figure 5. Phylogenetic Relationship and Expression Pattern of O11.

(A) Phylogenetic relationships of O11 and its homologs in plants. Distances were estimated using the neighbor-joining algorithm. The numbers at the nodes (100) represent the percentage of 1000 bootstraps. The scale bar indicates the average number of amino acid substitutions per site. The *Physcomitrella patens* homologous protein was used as an outgroup.

(B) and **(C)** RT-qPCR **(B)** and immunoblot **(C)** analysis of O11 in various tissues and developing kernels. All tissues (root, stem, third leaf, tassel, silk, husk, and ear) were collected from the V12 stage of field-cultivated W22 plants. The kernel samples were collected at different developmental stages, as indicated by days after pollination (DAP). The pericarp (PE), embryo (EMB), and endosperm (En) samples in **(C)** were harvested at 15 DAP. For RT-qPCR, transcript levels were normalized according to *Actin*. For immunoblot analysis, antitubulin was used as a loading control.

metabolic process (GO: 0044262, P value: 7.1E-06), and 29 DEGs were identified in this GO classification. The 29 DEGs were functionally clustered into two major categories: carbohydrate catabolic process (18 DEGs) and carbohydrate biosynthetic process (9 DEGs). Approximately 83% DEGs involved in the carbohydrate catabolic process were significantly upregulated. In addition, *Brittle-2* (*Bt2*; *GRMZM2G068506*) was among DEGs involved in carbohydrate biosynthetic process and was found to be significantly downregulated in *o11* kernels (fold change = −1.71). *Bt2* encodes the small subunit of maize endosperm ADP-glucose pyrophosphorylase (AGPase), which is considered to be a rate-limiting enzyme in starch biosynthesis (Dickinson and Preiss, 1969; Preiss et al., 1990). Thus, *o11* kernels exhibit increased expression of genes functioning in the carbohydrate catabolic process and decreased expression of key gene (e.g., *Bt2*) in starch biosynthesis.

Regarding amino acid metabolic processes, 30 DEGs (GO: 0006520, P value: 3.7E-06) were functionally clustered into three categories: amino acid biosynthetic process, amino acid catabolic process, and amino acid interconversion. Most DEGs involved in these processes were upregulated, suggesting that *o11* has a more active amino acid metabolism compared with the wild type.

Response to stress process was also affected in *o11* (GO: 0006950, P value: 0.0011), as 64 DEGs were identified. Over half of the DEGs in this cluster (33 DEGs) were involved in response to cold. Other DEGs were related to multiple types of stress response pathways, such as the response to biotic stress, oxidative stress, or DNA damage stimuli.

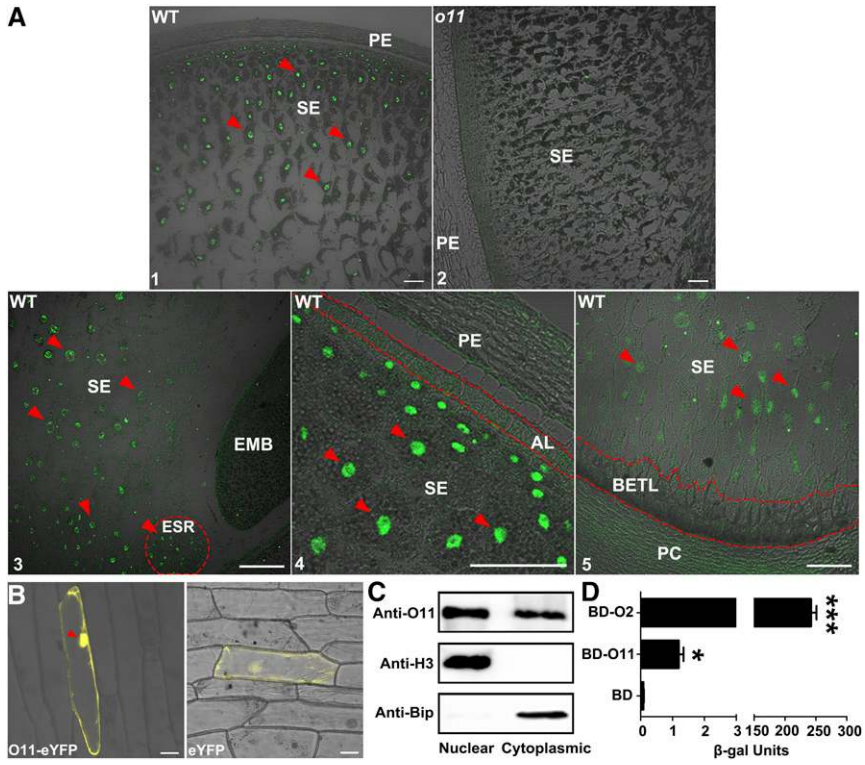

Figure 6. Subcellular Localization and Transactivation Analysis of O11.

(A) Immunofluorescence assays using an O11-specific antibody in 12-DAP wild-type and *o11* kernels. O11 immunofluorescence signals for the SE region are presented in a wild type kernel (subpanel 1) using an *o11* kernel as a negative control (subpanel 2). Immunofluorescence signals for the ESR, AL, and BETL in wild-type kernels are presented in subpanels 3 to 5, respectively. The red dotted cycle in subpanel 3 highlights the ESR region; red dotted lines in subpanels 4 and 5 highlight the AL and BETL regions, respectively. Red arrowheads indicate some typical O11 immunolabeling signals. PE, pericarp; PC, placento-chalazal region. Bars = 100 μm.

(B) Subcellular localization of O11-eYFP in *Nicotiana benthamiana*. The *eYFP* coding sequence was fused to the 3′ end of *O11*. The construct was transformed into *Agrobacterium tumefaciens* and transiently expressed in *N. benthamiana* leaves. The eYFP protein alone was used as a negative control. The red arrowhead indicates the nucleus. Bars = 50 μm.

(C) Nuclear and cytoplasmic fraction proteins obtained from 15 DAP W22 kernels were analyzed by immunoblotting with antibodies against O11, histone3 (H3; nuclear marker) and Bip (cytoplasm marker).

(D) Yeast transactivation assay of O11. The β-galactosidase activity resulting from TF transactivation was analyzed in yeast (yeast strain EGY48). BD (the pGBK-T7 empty vector) was used as a negative control. BD-O2 was used as a positive control. Error bars indicate ±SE ($n = 3$). *$P < 0.05$ and ***$P < 0.001$; Student's t test.

Mutation of O11 also affected the processes of nucleosome assembly and translation, which play fundamental roles in developmental processes. The 12 DEGs related to nucleosome assembly (GO: 0006334, P value: 0.0037) included multiple genes encoding histone proteins. In addition, 29 DEGs were related to translation (GO: 0006412, P value: 0.043), including numerous genes encoding ribosomal subunits and elongation factors.

ChIP-Seq Identifies Genes Directly Targeted by O11

To determine which DEGs are directly regulated by O11, chromatin immunoprecipitation sequencing (ChIP-seq) analysis was performed with an O11-specific antibody. The results shown in Supplemental Figure 7 validate the specificity of the O11 antibody. Cross-linked wild-type kernels and *o11* mutant kernels at 15 DAP were used for the ChIP-seq assay, and O11 binding sites were identified from consistent peaks generated by two independent biological replicates. A total of 9885 peaks distributed on 6033 genes were identified (Supplemental Data Set 4). We analyzed the distribution of O11 binding sites in the genome. Among all detected peaks, 66.5% were located in genic regions (−1 kb of the transcription start site [TSS] to +1 kb of the transcription termination site [TTS]) and 41% in core promoter regions (−1 kb to +100 bp of the TSS) (Figure 7B). In agreement with its predicted TF function, O11 binding sites were significantly concentrated within the 100 bp immediately upstream of TSSs (Figure 7C).

De novo discovery of the enriched motifs in the binding sites of the genic regions identified the G-box (CACGTG) as the top-scoring motif (52%, E-value = 2.5E-251) (Figure 7D). To test whether the G-box mediates transcriptional regulation of O11, a transient transcription dual-luciferase assay (dual-LUC assay) was performed using the promoters of potential O11 targets (*GRMZM2G102605* and *GRMZM2G019819*) (Supplemental Figures 8B to 8D). These targets were selected based on the

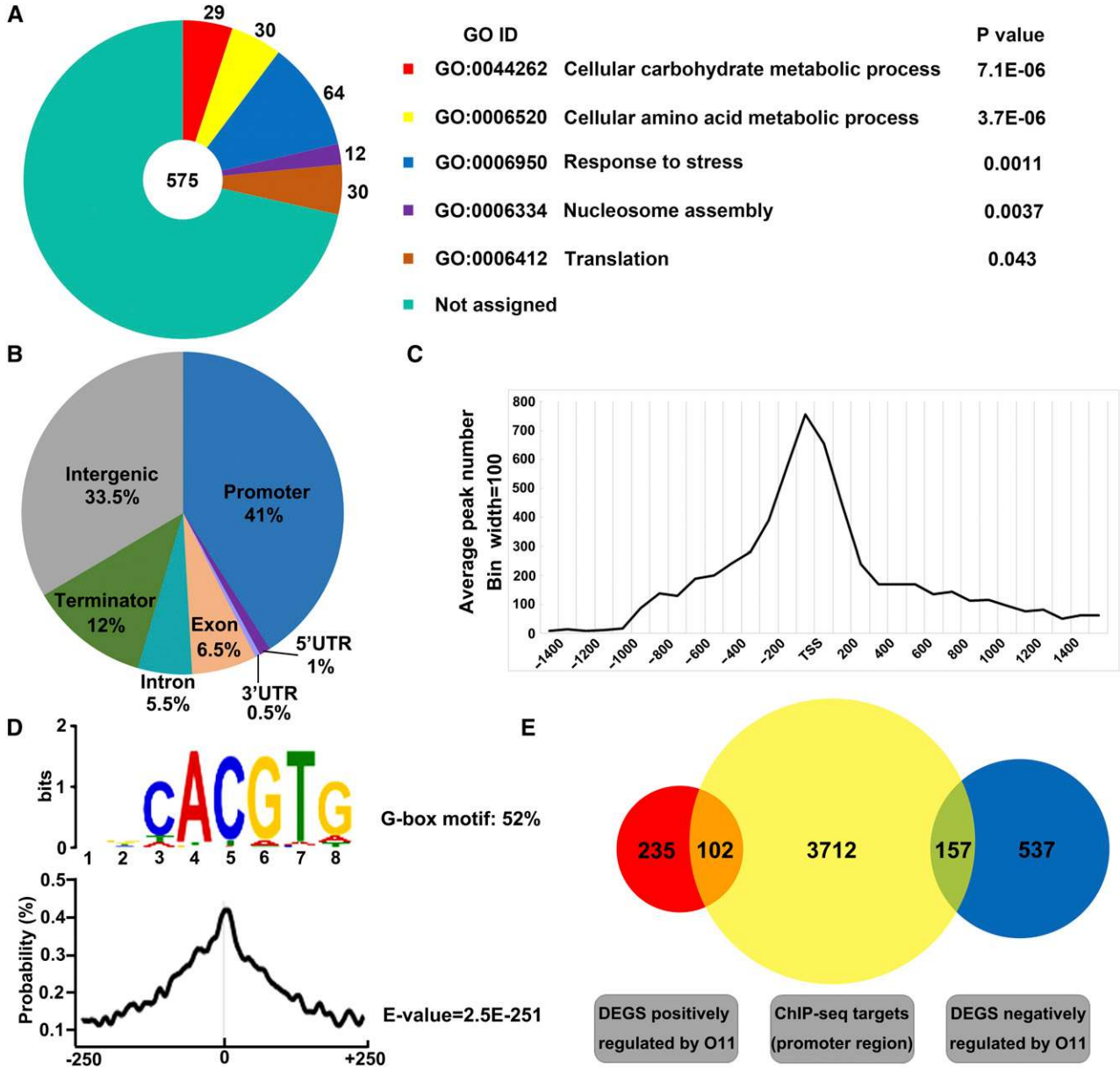

Figure 7. GO Classification of DEGs from RNA-Seq Analysis and Genome-Wide Binding Profiles from ChIP-Seq Analysis.

(A) GO classification of DEGs from *o11* RNA-seq analysis. The number of genes classified within each GO term as well as its P value are shown. In total, 575 genes were functionally annotated and classified using the GO database. E indicates 10 raised to a power in scientific notation.

(B) Distribution of O11 binding regions in the maize genome. Promoter region, −1 kb to +100 bp of the TSS; terminator, −100 bp to +1 kb of the TTS; intergenic region, 1 kb upstream of the TSS or 1 kb downstream of the TTS.

(C) Distribution of O11 binding sites per 100 bp bin corresponding to the −1500- to +1500-bp region flanking the TSS. The O11 binding sites are significantly concentrated in the 100 bp immediately upstream of the TSS.

(D) O11 binding motif identified by MEME-ChIP in the 500 bp flanking sequences around the genic peak summits and the density plot of this motif around the summits of the peaks. The "CACGTG" (G-box) motif was identified as the most prominent O11 binding motif (52%) (upper panel). In the lower panel, the *x* axis indicates the position of the binding motif in the sequence, and the *y* axis indicates the probability of the identified motif. The E-value is the enrichment P value times the number of candidate motifs tested. The enrichment P value was calculated using Fisher's exact test. E indicates 10 raised to a power in scientific notation.

(E) Venn diagram showing the overlap of 3971 genes bound by O11 in the promoter region to the 1031 DEGs identified from *o11* RNA-seq data (337 DEGs positively regulated by O11 and 694 DEGs negatively regulated by O11). Genes in the overlapping regions were identified as potential O11-targeted genes positively or negatively regulated by O11.

Table 1. Functional Classification of High-Confidence O11 Targets

Gene ID	Description	Fold Change	P Value
O11 targets involved in cellular carbohydrate metabolic process			
GRMZM2G130043	Starch synthase 5 (SS5)	−3.07	2.15E-02
GRMZM2G152686	Pyruvate kinase, ZmPKp-β1	−4.74	3.00E-14
GRMZM2G046804	Glyceraldehyde-3-phosphate dehydrogenase, GAPDH	1.62	3.00E-25
GRMZM5G833389	2,3-Bisphosphoglycerate-independent phosphoglycerate mutase	1.52	8.00E-05
GRMZM2G052844	6-Phosphofructokinase	1.99	1.00E-05
GRMZM2G442658	Alcohol dehydrogenase 1, ADH1	1.66	5.00E-42
GRMZM2G130440	Aldehyde dehydrogenase, ALDH	2.00	3.00E-32
GRMZM2G122172	Aldehyde dehydrogenase, ALDH	17.20	6.00E-06
GRMZM2G018820	Glycerophosphodiester phosphodiesterase	1.68	7.00E-14
GRMZM2G122277	Cellulose synthase-like family protein	1.76	4.37E-02
O11 targets involved in response to stress			
GRMZM2G392863	Low molecular weight cysteine-rich 69a	−2.25	5.00E-279
GRMZM2G130868	Uncharacterized protein	−2.62	2.00E-04
GRMZM2G046532	Low molecular weight cysteine-rich 69b	−2.24	7.00E-106
GRMZM2G155954	Uncharacterized protein	−2.08	5.00E-04
GRMZM2G075655	DNA repair ATPase-related protein (DRAP)	−1.88	2.10E-03
GRMZM2G155323	L-*O*-methylthreonine resistant 1, threonine dehydratase (ZmOMR1)	−1.84	1.55E-02
GRMZM2G079956	Bcl-2-associated athanogene protein (BAG)	1.54	4.49E-02
AC189750.4_FG004	Adenosine 5′-phosphosulfate reductase 1	1.54	2.45E-02
GRMZM2G093272	USP family protein	1.60	4.00E-04
GRMZM2G405581	Peroxidase superfamily protein	1.62	3.16E-02
GRMZM2G407146	Wound-responsive family protein	1.76	3.00E-10
GRMZM2G105901	Uncharacterized protein	1.97	6.00E-04
GRMZM2G015605	Low-temperature and salt-responsive protein family	1.75	4.00E-07
GRMZM2G045664	Late embryogenesis abundant protein	1.80	2.80E-03
GRMZM2G103812	Selenium-binding protein 2	1.81	2.00E-14
GRMZM2G170338	Glutamine amidotransferase type 1	1.67	8.00E-04
GRMZM2G080183	Peroxidase	2.06	4.51E-02
GRMZM2G037411	Pectin lyase-like superfamily protein	2.67	1.00E-12
GRMZM2G380088	Cytidine deaminase	2.78	1.00E-05
GRMZM2G075974	Glutamine amidotransferase type 1	2.47	8.00E-07
GRMZM2G181371	Uncharacterized protein	3.10	2.00E-18
O11 targets that are ESR specific			
GRMZM2G031613	Subtilisin-like protease (SLP)	−2.50	6.00E-04
GRMZM2G093316	ZmYODA, MAPKK kinase	−3.09	1.02E-02
GRMZM2G042639	Glutathione transferase	2.98	1.67E-02
GRMZM2G168365	ZmSAG29	5.08	9.00E-11
GRMZM2G064605	Thaumatin, pathogenesis-related	20.10	6.00E-44
O11 targets that encode transcription factors			
GRMZM2G015534	O2	1.82	3.00E-19
GRMZM2G146283	Dof zinc finger transcription factor (PBF)	−1.55	1.25E-02
GRMZM5G884137	Indeterminate domain (IDD) TF (NKD2)	1.89	9.00E-04
GRMZM2G137502	ZmDOF3	−2.10	2.30E-03
GRMZM2G139073	SILKY1	−2.09	3.24E-02
GRMZM2G339751	(WOX2) WUSCHEL related homeobox 2	−2.34	2.16E-02
GRMZM2G046885	ZmSVP	3.07	7.00E-04
GRMZM2G320549	ZmAGL19	−4.11	2.80E-03
GRMZM2G064775	ZmJAZ1, Jasmonate ZIM-domain 1	1.98	1.00E-12
GRMZM2G125653	ZmWRKY53	8.85	9.00E-04
GRMZM2G117513	ZIM24, ZIM-transcription factor 24	−1.95	3.01E-02
GRMZM2G386674	LBD-transcription factor 33	1.58	2.74E-02
GRMZM2G091201	MYB-related transcription factor 13	1.58	1.11E-02
GRMZM2G011932	Transcription factor GBF1	1.81	3.30E-03
GRMZM2G103647	bZIP17, bZIP-transcription factor 17	2.41	1.00E-14
GRMZM2G100583	NAC75, NAC-transcription factor 75	3.42	1.25E-02

(Continued)

Table 1. (continued).

Gene ID	Description	Fold Change	P Value
GRMZM2G127379	NAC25, NAC-transcription factor 25	3.65	1.43E-02
GRMZM2G090595	IDDP10, indeterminate domain protein10	−2.12	2.00E-04
AC198366.3_FG004	GRAS29, GRAS-transcription factor 29	3.82	1.43E-02
GRMZM2G376061	C2H2-type zinc finger family TF	7.83	1.74E-02
GRMZM2G112799	C2H2-type zinc finger family TF	8.05	1.74E-02

presence of the G-box motif under the summit of the O11 binding sites and their downregulation in *o11*. The same promoters with the G-box replaced by "AAAAAA" were used as a control (Supplemental Figure 8B). O11 significantly activated these promoters, whereas G-box mutation dramatically decreased or eliminated transactivation by O11 (Supplemental Figures 8C and 8D). Our data indicate that O11 can transactivate the promoters of its target genes and that full transactivation depends on the presence of the G-box binding motif.

To explore the direct regulatory function of O11 across the genome, all genes directly bound by O11 in promoter regions (3971 genes) were analyzed using the GO database (http://bioinfo.cau.edu.cn/agriGO/). Among them, 2086 genes were functionally annotated and classified into seven GO terms under four biological processes: metabolic process (cellular carbohydrate metabolic process [GO: 0044262, P value: 6.50E-05]); stress response process (response to stress [GO: 0006950, P value: 6.60E-10] and response to chemical stimulus [GO: 0042221, P value: 1.10E-14]); developmental process (organ development [GO: 0048513, P value: 8.00E-07] and signal transduction [GO:0007165, P value: 4.30E-08]); and gene expression (regulation of transcription [GO:0045449, P value: 1.20-11E] process and post-translational protein modification [GO:0043687, P value: 2.40E-06]) (Supplemental Figure 9 and Supplemental Data Set 5). To obtain high-confidence targets that are primarily regulated by O11, we compared 3971 genes bound by O11 in the promoter region to the 1031 DEGs from the *o11* RNA-seq data. In total, 259 high-confidence potential targets of O11 were identified (Figure 7E; Supplemental Data Set 6).

O11 Directly Regulates Genes Involved in Carbohydrate Metabolism and Stress Responses

To explore the biological functions of O11, the 259 high-confidence potential targets were functionally annotated and classified using the GO database (http://bioinfo.cau.edu.cn/agriGO/), and two GO clusters were generated. One GO cluster was cellular carbohydrate metabolic process (GO: 0044262, P value = 0.041) and was complemented by the MapMan database (Table 1). *Starch synthase5* (*Ss5*) and nine genes involved in glycolysis, the tricarboxylic acid (TCA) cycle, fermentation, and other carbohydrate metabolic process were found to be direct targets of O11, including those encoding pyruvate kinase (*ZmPKp-β1*), glyceraldehyde-3-phosphate dehydrogenase (*Gpc1*), and 6-phosphofructokinase and alcohol dehydrogenase 1 (*Adh1*). Loss of function of O11 significantly downregulated *Ss5* and upregulated most carbohydrate metabolic genes (Table 1). Dual-luciferase (LUC) assays using the promoters of down-regulated *Ss5* and *ZmPKp-β1* in this cluster were performed, and the results showed that O11 specifically activates the *Ss5* and *ZmPKp-β1* promoters (Figures 8A and 8B). These results demonstrate that O11 directly regulates genes involved in carbohydrate metabolism.

The contents of the intermediate metabolites of glycolysis and the TCA cycle were also analyzed in wild-type and *o11* developing endosperm at 15 DAP by gas chromatography-mass spectrometry (GC-MS). The contents of glucose-6-phosphate, citrate, succinate, and fumarate, key intermediate metabolites in glycolysis and the TCA cycle pathways, were significantly reduced in *o11* (Figure 9; Supplemental Table 1), suggesting that the loss of O11 function significantly affects glycolysis and TCA metabolism in the maize endosperm.

The other GO cluster identified was response to stress (GO: 0006950, P value = 0.0048), and 21 targets were annotated as stress response genes (Table 1). Target genes involved in this category included proteins of related functions, such as amino acid metabolism, DNA repair, apoptosis regulation, and cytokinin signaling. Four of the six downregulated targets had functional annotations (L-*O*-methylthreonine resistant1 [ZmOMR1], DNA repair ATPase-related protein [DRAP; GRMZM2G075655], and two low molecular weight cysteine-rich [LCR] 69 proteins [LCR 69a and LCR 69b]). These four targets were further examined in dual-LUC assays, and the results showed that activation of all these promoters was specifically induced by O11 (Figures 8C to 8F). These results demonstrate that O11 directly regulates genes involved in responses to stress.

O11 Regulates Genes Specifically Expressed in the ESR

The ortholog of O11 in Arabidopsis, AtZOU, plays critical roles in the ESR in regulating endosperm breakdown and embryo epidermal development (Yang et al., 2008; Xing et al., 2013; Denay et al., 2014; Fourquin et al., 2016). Yang et al. (2008) showed that *zou* endosperm fails to separate from the embryo, restricting embryo expansion and resulting in the production of shriveled, collapsed seeds. Analogous to the morphological defects observed in *atzou*, the *o11* ESR displayed similar adhesion to the embryo (Figure 1F). RNA-seq analysis of laser-capture microdissected compartments of the maize kernel (LCM RNA-seq) has been performed, and ESR-specific genes with preferential ESR expression were identified (Zhan et al., 2015). We overlapped the reported ESR-specific genes with the 259 high-confidence potential targets of O11, revealing five ESR-specific genes regulated by O11 (Table 1). One of these genes, *ZmYoda*, is the ortholog of Arabidopsis *YODA* (*AtYODA*), which encodes a mitogen-activated protein kinase kinase kinase (MAPKKK). AtYODA was previously reported to be a key component in the MAPK pathway, regulating embryo differentiation and

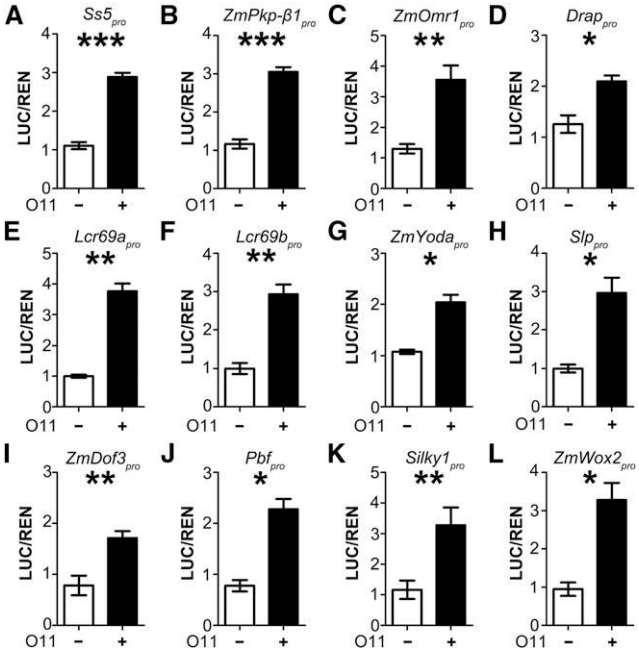

Figure 8. Dual-LUC Assay with O11 Potential Targets.

Relative reporter activities (LUC/REN) of O11 to its potential target promoters (1 kb upstream sequence of the start codon) in *N. benthamiana* plants. Relative LUC activities (normalized to the REN activity) are shown. The tested promoters are indicated above each panel. Overexpressed O11 protein was used as the effector. Error bars indicate ±SE ($n = 3$). *P < 0.05, **P < 0.01, and ***P < 0.001; Student's *t* test. −, without O11 present; +, with O11 present.

stomatal development in Arabidopsis (Bergmann et al., 2004; Lukowitz et al., 2004; Wang et al., 2007; Kim et al., 2012). In maize, *ZmYoda* is significantly downregulated (fold change = −3.1) due to O11 loss of function (Table 1). Another ESR-specific target, *ZmSag29*, encodes a hexose and sucrose transporter, the transcript of which was increased 5.1-fold in the *o11* mutant. *ZmSag29* is the ortholog of *SENESCENCE-ASSOCIATED GENE29* in Arabidopsis (*AtSAG29*), and it is reported that overexpression of *AtSAG29* accelerates senescence (Seo et al., 2011). Dual-LUC assays using the promoters of down-regulated target genes (*ZmYoda* and a subtilisin-like protease [*Slp*]) were performed, and the results demonstrated that O11 can activate the promoters of both *ZmYoda* and *Slp* (Figures 8G and 8H). All these data indicate that O11 regulates ESR-specific genes in the maize endosperm.

O11 Regulates Key TFs and Coregulates *cyPpdks* with O2

Approximately 8% (21 of 259) of the O11 high-confidence potential targets obtained encoded TFs (Table 1), including NKD2, ZmDOF3, PBF, and O2, which are known key TFs that play important roles in both endosperm development and nutrient accumulation. NKD2 regulates a series of biological processes in endosperm development, and ZmDOF3 is a key regulator of starch accumulation and endosperm development (Yi et al., 2015; Gontarek et al., 2016; Qi et al., 2017). O2 and PBF reportedly to play pivotal roles in zein protein and starch accumulation (Vicente-Carbajosa et al., 1997; Wu and Messing, 2012; Li et al., 2015; Zhang et al., 2016). Moreover, *Silky1* and *ZmWox2* are direct targets of O11 and might function in endosperm development, as SILKY1 was previously shown to be a key regulator of maize floral organ development (Ambrose et al., 2000), and AtWOX2, the ortholog of ZmWOX2 in Arabidopsis, is involved in embryo apical patterning and cotyledon development (Wu et al., 2007; Breuninger et al., 2008; Lie et al., 2012). As downregulated targets, the promoters of the genes encoding ZmDOF3, PBF, SILKY1, and ZmWOX2 were selected for dual-LUC assays, and the results showed all to be specifically induced by O11 (Figures 8I to 8L).

O2 was increased both at the mRNA (1.82-fold) and protein levels in *o11* (Figure 10A). To investigate the regulatory relationship between O11 and O2 in the developing maize endosperm, we overlapped all 2564 peaks from the O2 ChIP-seq data (Li et al., 2015) with the total 9885 peaks of O11, with 247 overlapping peaks observed (9.6% overlap ratio for O2; 2.5% overlap ratio for O11) (Figure 10B; Supplemental Data Set 7). A total of 171 of the 247 peaks fell into 169 genes, and 73% of them (123 genes) were bound in the promoter regions (Figure 10C). In total, 101 common targets were bound in promoter regions and expressed in the endosperm according to the RNA-seq data of *o11* and *o2* (Supplemental Data Set 7). Among them, nine targets were transcriptionally altered in both *o11* and *o2* (P value < 0.05). Interestingly, seven of the nine targets were downregulated in *o2* but upregulated in *o11*, including both *cyPpdk1* and *cyPpdk2* (Supplemental Data Set 8), suggesting that O11 and O2 have antagonistic actions in regulating their common targets.

We then performed dual-LUC assays using the promoters of *cyPpdk1* and *cyPpdk2* (Figures 10D and 10E). O2 strongly activated these promoters, whereas O11 showed no significant activation. When O2 and O11 were both present, transactivation of

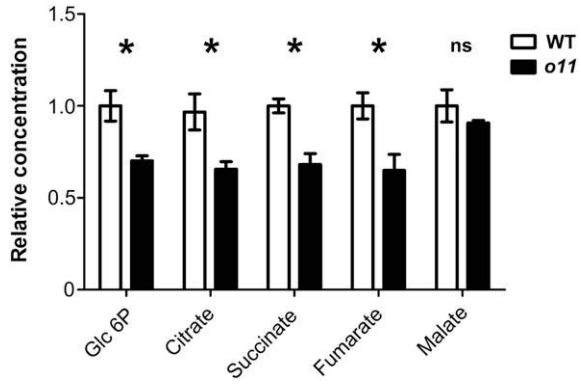

Figure 9. Relative Content of Carbohydrate Metabolites in Wild-Type and *o11* Endosperm.

Peak areas of wild-type and *o11* metabolites were normalized by the internal standard ribitol, which was derivatized concomitantly with the tissue samples, and were compared with the mean peak area calculated from the corresponding wild type. Three biological replicates were produced from three independently pooled wild-type or *o11* endosperm. For peak area of the carbohydrate metabolites, see Supplemental Table 1. Error bars indicate ±SE ($n = 3$). *P < 0.05; ns, not significant; Student's *t* test.

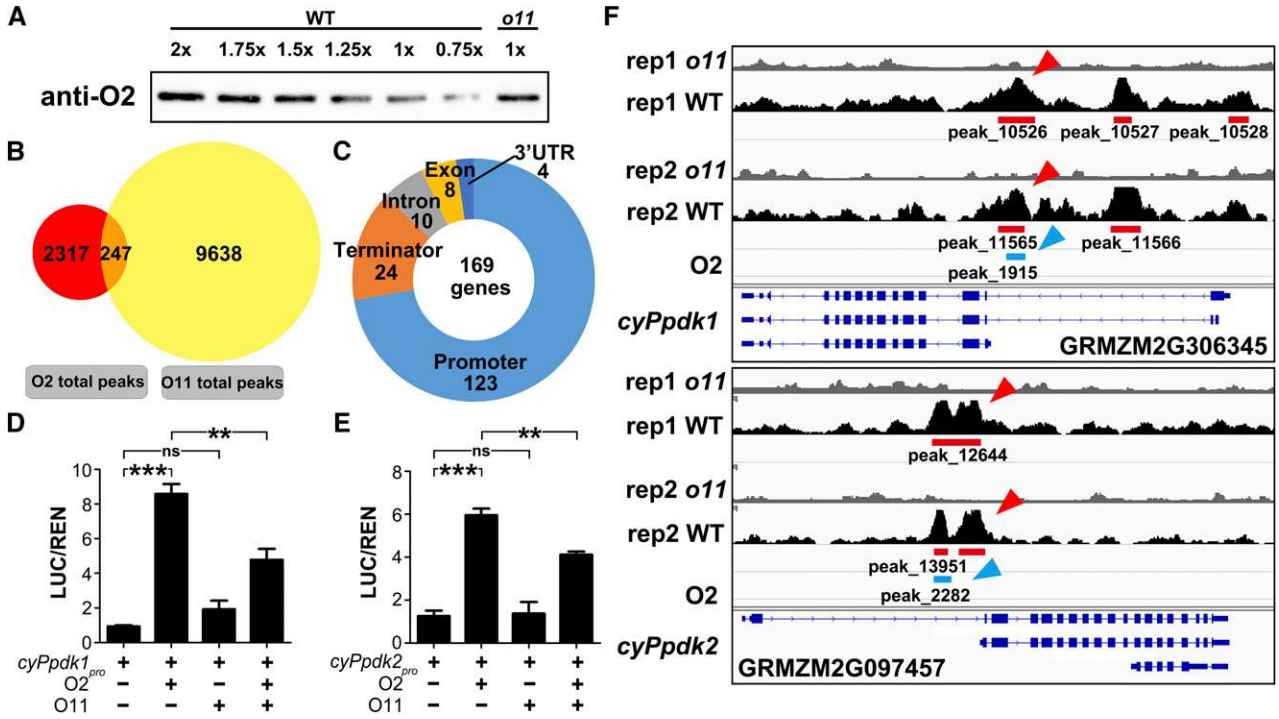

Figure 10. The Regulatory Relationship between O11 and O2 in the Maize Endosperm.

(A) O2 protein levels in wild-type and *o11* mutant kernels. Total protein extracts obtained from wild-type and *o11* kernels at 15 DAP were separated by 10% SDS-PAGE and blotted onto a nitrocellulose membrane. For the 1× wild-type and *o11* samples, ~30 μg protein was loaded. For the wild-type sample, a 2× to 0.75× dilution series was performed. Immunoblotting was performed with an O2 antibody, and signal detection was performed by chemiluminescence using a chemiluminescence analyzer (Tanon 5200).

(B) Venn diagram showing the overlap of all 2564 peaks identified from the O2 ChIP-seq data with the 9885 peaks identified from the O11 ChIP-seq data. Peaks in the overlapping regions were identified as common peaks bound by both O11 and O2 across the genome.

(C) Distribution of overlapping genes bound by both O11 and O2 in the maize genome. Promoter region, −1 kb to +100 bp of the TSS; terminator, −100 bp to +1 kb of the TTS.

(D) and **(E)** Relative reporter activities (LUC/REN) of different effectors (O2 or/and O11) with the promoters of *cyPpdk1* or *cyPpdk2* in *N. benthamiana* plants. Relative LUC activities (normalized to REN activity) are shown. Error bars indicate ±SE ($n = 3$). **$P < 0.01$ and ***$P < 0.001$; ns, not significant; Student's *t* test.

(F) Distributions of O11 and O2 binding sites for *cyPpdk1* (*GRMZM2G306345*) and *cyPpdk2* (*GRMZM2G097457*) loci, as shown in Integrated Genome Browser. Red lines (O11) or blue lines (O2) indicate significant peaks calculated by MACS2. Red or blue arrowheads indicate overlapping peaks of O11 or O2, respectively. The O11 binding sites were obtained from two independent biological replicates (rep1 and rep2).

the *cyPpdk1* or *cyPpdk2* promoter was significantly lower than when O2 was present alone (Figures 10D and 10E). These results demonstrate that O11 might function as a repressor of O2. According to our ChIP-seq data, the O11 binding sites completely cover the O2 binding sites in both *cyPpdk1* and *cyPpdk2* (Figure 10F). Yeast two-hybrid (Y2H) assay and luciferase complementation image (LCI) assay results indicated that O11 and O2 do not interact with each other (Supplemental Figure 10). Therefore, O11 possibly prevents O2 from binding to the same binding sites in the promoters of *cyPpdk1* and *cyPpdk2* in vivo. The repression ability of O11 might occur through binding site competition with other strong activators.

ZmICE1 Coordinates Regulation of Stress Response Genes and *ZmYoda* with O11

As bHLH TFs tend to form homo- or heterodimers to regulate their targets, a Y2H screening assay was performed to identify O11-interacting proteins. After screening ~8 million recombinant cDNA clones, we identified 35 putative O11-interacting proteins (Supplemental Table 2). Eighteen proteins with independent positive clones from the Y2H screening were further analyzed by an LCI assay (Figure 11). Six bHLH-type TFs, including Inducer of CBF Expression 1 in maize (ZmICE1 or ZmICEa, GRMZM25173534) (Grimault et al., 2015), as well as five non-TF proteins (two aspartate kinases, two Golgi trafficking-related proteins and one plant-specific protein) passed LCI interacting tests (Figure 11).

AtICE1 in Arabidopsis has been identified as a direct regulator of C-repeat binding factors (CBFs) in the response to cold stress (Chinnusamy et al., 2003). ZmICE1 (ZmICEa) has been reported to have a stronger interaction with O11 (ZmZOU) than the other two homologs (ZmICEb and ZmICEc), and these interactions can transactivate target gene promoters from Arabidopsis (Grimault et al., 2015). Among the direct targets of O11 involved in the response to stress, 13 are annotated as genes related to the

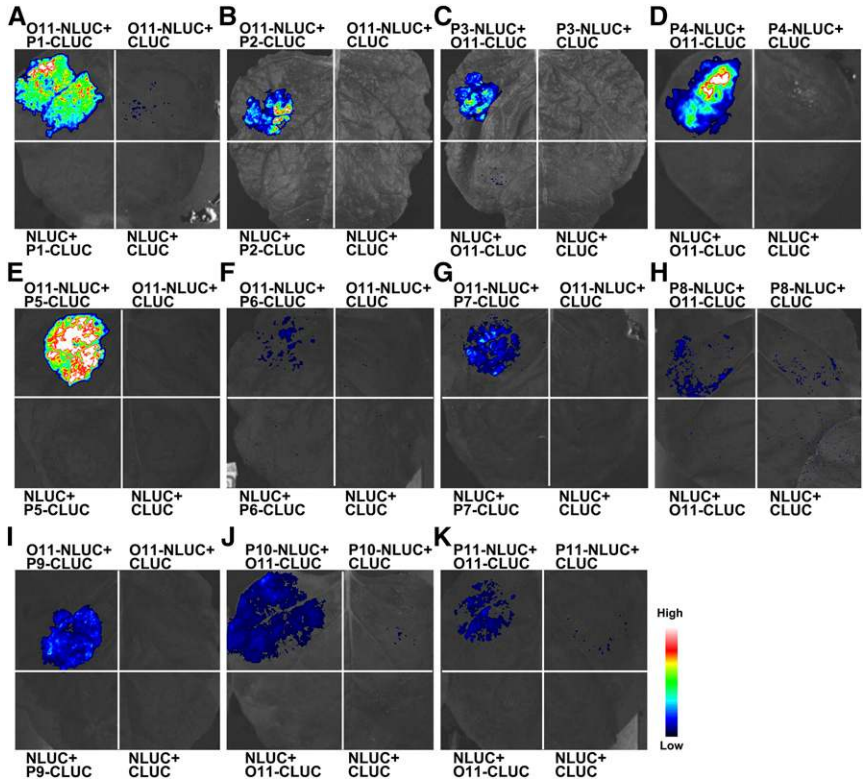

Figure 11. Interactions between O11 and Y2H-Identified Candidate Proteins, as Tested by the LCI Assay in *N. benthamiana*.

Result of the LCI assay between O11 and Y2H-identified proteins. P1 to P11 represent the proteins encoded by *GRMZM2G089501* **(A)**, *GRMZM2G173534* (*ZmICE1*) **(B)**, *GRMZM2G030123* **(C)**, *GRMZM2G083749* **(D)**, *AC215201.3_FG008* **(E)**, *GRMZM2G069408* **(F)**, *GRMZM2G024686* **(G)**, *GRMZM2G300862* **(H)**, *GRMZM2G116626* **(I)**, *GRMZM2G165949* **(J)**, and *GRMZM2G118743* **(K)**. For each panel, the upper-left section shows the interaction signal between O11 and the Y2H-identified protein; the other three sections show the signals of the negative controls. The specific combinations used for each interaction are labeled next to each panel. The fluorescence signal intensity represents their interaction activities.

response to cold. To assess whether O11 and ZmICE1 can coregulate these 13 cold stress response targets in vivo, ChIP-qPCR was performed using an antibody against ZmICE1 (the specificity and immunoprecipitation effectivity of ZmICE1 antibody are shown in Supplemental Figure 11). Eight targets showed enrichment in ZmICE1 ChIP samples (Figure 12A), suggesting that O11 and ZmICE1 coregulate a portion of cold-stress response genes in vivo. A dual-LUC assay was performed with one of the common cold-stress response targets: *ZmOmr1*. The *ZmOmr1*$_{pro}$*-LUC* reporter was transiently expressed together with O11 or ZmICE1 or both in *N. benthamiana* leaves. O11 or ZmICE1 alone was able to activate the *ZmOmr1*$_{pro}$*-LUC* reporter (Figure 12B), the expression level of which was significantly enhanced when O11 was combined with ZmICE1 (Figure 12B). These results suggest that O11 and ZmICE1 can coactivate their common targets.

It is reported that AtICE1 also controls stomatal differentiation (Kanaoka et al., 2008). As AtYODA acts as a molecular switch in stomatal differentiation and O11 interacts with ZmICE1 and directly regulates *ZmYoda*, we speculated that ZmICE1 might also be involved in regulating *ZmYoda*. We thus performed ChIP-qPCR with a ZmICE1-specific antibody, and the results showed that ZmICE1 binds to the promoter of *ZmYoda* (Figure 12C). A dual-LUC assay was performed, and both O11 and ZmICE1 were found to activate the *ZmYoda*$_{pro}$*-LUC* reporter alone (Figure 12D). In contrast to the results reported above, the expression level of the *ZmYoda*$_{pro}$*-LUC* reporter was not significantly enhanced when O11 and ZmICE1 were coexpressed (Figure 12D), suggesting that they coregulate *ZmYoda*, but not in a cotransactivational manner.

DISCUSSION

O11 Is a bHLH TF with Potential New Functions in Maize

The strategies to store nutrients in the seeds differ dramatically between monocotyledonous and dicotyledonous species. In the seeds of monocotyledonous species, nutrients are usually stored in the endosperm, with abundant accumulation until maturation. By contrast, the endosperm in the seeds of dicotyledonous species (such as Arabidopsis) is absorbed by the cotyledons during the course of development, leaving only a single layer of endosperm cells; thus, nutrients are stored in the cotyledons (Olsen, 2004). AtZOU, the ortholog of O11 in Arabidopsis, plays

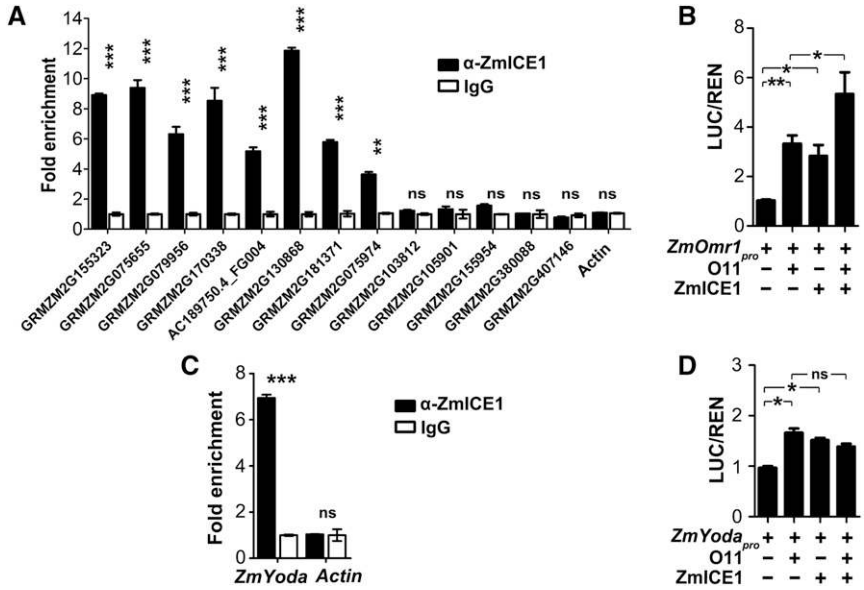

Figure 12. ZmICE1 Coregulates Stress Response Genes and *ZmYoda* with O11.

(A) and **(C)** ChIP-qPCR assays examining the in vivo binding activity of ZmICE1 to the promoters of the cold-stress response targets of O11 **(A)** or *ZmYoda* **(C)**. Primers for the promoter fragments of the 13 cold-stress response targets of O11 **(A)** and *ZmYoda* **(C)** were used to detect enrichment of target sequences in the ChIP products of ZmICE1; ChIP products of IgG were used as a negative control. *Actin* was used as an internal control. Error bars indicate ±SE ($n = 3$). **P < 0.01 and ***P < 0.001; ns, not significant; Student's *t* test.

(B) and **(D)** Relative reporter activity (LUC/REN) of different effectors (O11 or/and ZmICE1) with the promoters of *ZmOmr1* **(B)** or *ZmYoda* **(D)** in *N. benthamiana* plants. Relative LUC activities (normalized to the REN activity) are shown. Error bars indicate ±SE ($n = 3$). *P < 0.05 and **P < 0.01; ns, not significant; Student's *t* test.

critical roles in endosperm breakdown and embryo epidermal development (Yang et al., 2008; Xing et al., 2013; Denay et al., 2014; Fourquin et al., 2016). Our analysis revealed significant differences between these orthologs in terms of their protein sequence, expressed compartments, and biological function. First, O11 contains an additional 300 amino acids at its N terminus (Supplemental Figure 6). Moreover, except for the bHLH domain, sequence similarity between the orthologs is quite low. Thus, the orthologs are in two clades of the phylogenetic tree (Figure 5A). Second, expression of *AtZOU* is restricted to the ESR region (Yang et al., 2008), but according to our immunofluorescence analysis, O11 accumulates in both the ESR and the SE (Figure 6A). LCM RNA-seq data (Zhan et al., 2015) (Supplemental Table 3) and qPCR results from another study (Grimault et al., 2015) support our observations.

O11 Is a Central Regulator Linking Maize Endosperm Development, Metabolism, and Stress Response

To explore the biological functions of O11, we investigated global transcriptional changes caused by O11 loss of function and found pleiotropic effects in *o11*, including cellular metabolic processes, developmental processes and stress responses (Figure 7A). Furthermore, to examine direct targets of transcriptional regulation, genome-wide DNA binding sites of O11 were determined by ChIP-seq analysis in developing maize kernels (Figures 7B to 7E). We identified the G-box as the dominant binding motif for O11 (Figure 7D), which is consistent with previous studies of other bHLH TFs (Oh et al., 2009, 2012; Zhang et al., 2013). We performed electrophoretic mobility shift assays to evaluate the binding ability of O11 to the G-box but failed to observe a band shift (Supplemental Figure 8A). We speculate that this result might be because prokaryotic expression of O11 results in the absence of modifications that are essential for DNA binding, e.g., phosphorylation (Klimczak et al., 1992). O11 exhibits dual activator/repressor activity profiles (Figure 7E). O11 activates its targets via transactivation (Figure 8) and might also coactivate common targets with interacting proteins (e.g., ZmICE1) (Figure 12B). The transcriptional repression ability of O11 might be due to its binding to the same regions of other strong activators (e.g., O2) (Figures 10D to 10F), which is defined as a passive repressor (Krogan and Long, 2009).

Through comprehensive transcriptome and DNA binding site analysis, we found that O11 functions as a central regulator in the gene networks governing maize endosperm development, nutrient metabolism, and stress response (Figure 13). O11 not only regulates genes for key TFs in endosperm development (*Nkd2* and *ZmDof3*) but also controls key regulators of endosperm nutrient metabolism (*O2*, *Pbf*, and *cyPpdk1* and *-2*). Moreover, O11 is a direct activator of the upstream MAPKK kinase gene *ZmYoda*, suggesting that its regulatory function in endosperm development occurs through MAPK signaling. We also investigated the regulatory relationship between O11 and an interacting protein (ZmICE1), and the results showed that they might coregulate endosperm development and stress responses.

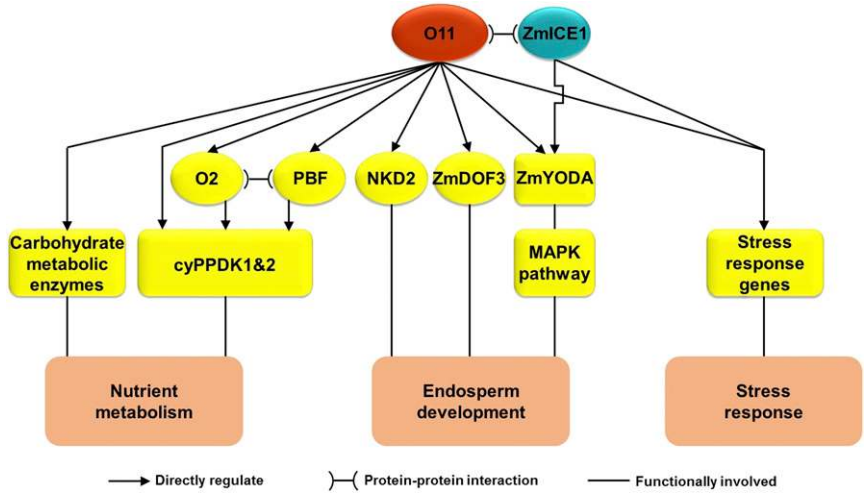

Figure 13. A Schematic Diagram of the Regulatory Network of O11 in Maize Endosperm.

O11 is in the central position of a regulatory network governing maize endosperm metabolism, development, and stress response. O11 regulates nutrient metabolism through directly regulating carbohydrate metabolic enzymes and the upstream regulators (such as O2 and PBF). O11 influences endosperm development through directly regulating key regulators in development (such as NKD2 and ZmDOF3). Meanwhile, O11 interacts with ZmICE1, and they coregulate endosperm development and stress response through directly regulating *ZmYoda*, a key switch in development, and stress response genes.

O11 Is a Key Regulator in Endosperm Nutrient Metabolism

o11 mutant kernels display a reduced and less vitreous (opaque) endosperm (Figures 1A to 1C). Consistently, the starch granules and PBs in the *o11* endosperm were smaller, and the total starch and protein contents per kernel were significantly decreased (Figures 2D and 2E). As starch accounts for ~75% of the dry weight of maize kernels, the reduced starch accumulation in *o11* endosperm should be responsible for its reduced endosperm. Numerous studies on opaque mutants have reported positive correlations between morphological alterations of PBs (*o1*, *o2*, *o6*, *o7*, and *o10*) or starch granules (*o5*) and opaque endosperm (Schmidt et al., 1987; Miclaus et al., 2011; Myers et al., 2011; Wang et al., 2011, 2012, 2014; Yao et al., 2016). Starch granules in normal endosperm cells appear to be tightly interwoven with a proteinaceous matrix largely composed of PBs (Wu and Messing, 2010), and alterations in PB or starch granule morphology would change a compact transparent endosperm into a loose opaque endosperm. Thus, we believe that the morphological changes observed for PBs and starch granules in *o11* endosperm cells are responsible for the opaque endosperm of *o11*.

Loss of function of O11 significantly affects transcription of genes related to cellular carbohydrate and amino acid metabolism, indicating the essential role of O11 in endosperm nutrient metabolism (Figure 7A). We found that O11 directly activates a starch synthase gene and represses those involved in glycolysis, the TCA cycle, and other carbohydrate metabolic process (Table 1); such changes would accelerate starch decomposition, revealing the positive roles of O11 in guaranteeing starch accumulation. O2 and PBF are both well-known TFs regulating expression of zein protein genes (Schmidt et al., 1987; Vicente-Carbajosa et al., 1997), and recent studies indicate that they are also involved in the endosperm's carbon and nitrogen metabolism (Li et al., 2015; Zhang et al., 2016). O11 directly regulates both O2 and PBF (Table 1), suggesting upstream regulatory roles for O11 in endosperm nutrient metabolism. Moreover, the *o11* endosperm showed a disrupted C/N ratio (Figure 2G). Previous studies have reported that cyPPDKs are key molecular switches in the endosperm starch/protein balance through inorganic PPi-dependent restriction of starch synthesis as well as through provision of substrates for amino acid synthesis (Sheen, 1991; Prioul et al., 2008; Manicacci et al., 2009). O11 directly binds to the promoters of *cyPpdk1* and *-2* (Figure 10F), and their expression is significantly altered in O11 loss-of-function mutants (Supplemental Data Set 8), suggesting that O11 is a key modulator in the starch/protein balance. Therefore, O11 is involved in multilayer transcriptional regulation of endosperm carbohydrate and amino acid metabolism. Indeed, mutation of O11 disrupts carbohydrate and amino acid metabolism, thereby affecting the accumulation and morphology of starch granules and PBs and, ultimately, resulting in the reduced and opaque endosperm of the *o11* mutant.

O11 Is a Key Regulator in Endosperm Development

Loss of function of O11 results in a reduced endosperm with developmental defects (Figure 1), indicating the critical roles of O11 in endosperm development. Our data show that O11 occupies the central position of a regulatory network in endosperm development. In addition to NKD2, ZmDOF3, and SILKY1, the three TFs encoded by the target genes of O11 (ZmWOX2, ZmSVP, and ZmAGL19) might also be involved in endosperm development (Table 1), as their orthologs in Arabidopsis are involved in embryo development, floral meristem differentiation, and floral transition, respectively (Hartmann et al., 2000; Schönrock et al., 2006; Wu et al., 2007; Breuninger et al., 2008; Lie et al., 2012; Gregis et al., 2013). Moreover, two O11-interacting bHLH TFs (ZmBIM and

ZmLHW) may also regulate endosperm development (Supplemental Table 2), as their orthologs are reported to function in the brassinosteroid signaling pathway and in root differentiation, respectively (Ohashi-Ito and Bergmann, 2007; Cifuentes-Esquivel et al., 2013).

Previous studies have demonstrated that loss of AtYODA function results in abnormal embryo differentiation and excess stomata in the epidermis, whereas overexpression of AtYODA suppresses embryonic development and eliminates stomata (Bergmann et al., 2004; Lukowitz et al., 2004; Wang et al., 2007; Kim et al., 2012). Thus, the YODA/MAPK cascade plays a major role in regulating both the polarity of asymmetric cell divisions of stomata and zygote development. Our data showed that O11 is a direct activator of *ZmYoda* (Figure 8G) and that loss of O11 function significantly downregulates *ZmYoda* transcription (Table 1), suggesting that the regulatory function of O11 in endosperm development occurs through the MAPK pathway. It has been reported that the number of fully differentiated stomata is reduced when *O11* is ectopically expressed in maize leaves (Grimault et al., 2015). The decrease in the number of stomata in O11-overexpressing leaves might also be due to excess transactivation of *ZmYoda* by O11. *ZmYoda* was found to be preferentially expressed in the ESR (Zhan et al., 2015) (Supplemental Table 3), suggesting that ZmYODA might also be involved in ESR differentiation by regulating asymmetric cell divisions.

The Role of O11 in Stress Responses

In addition to the central roles of O11 in regulating endosperm development, we unexpectedly found that O11 also participates in stress response regulation. Loss of function of O11 caused excessive transcriptional changes in stress response genes (Figure 7A). Moreover, target analysis showed that O11 directly regulates many stress response genes (Table 1), and many TF gene targets of O11 might be involved in the stress response (Table 1), such as *ZmJaz1* and *ZmWrky40*, which, according to the annotations of their orthologs from Arabidopsis, are considered to modulate stress responses (Hu et al., 2013; Xu et al., 2006).

A transcriptome study of the maize developing endosperm reported that stress response TFs (e.g., WRKY family TFs) are differentially expressed under normal conditions during endosperm development (Qu et al., 2016). AtICE1 is a key regulator in the response to cold stress and plays critical roles in stomatal development (Chinnusamy et al., 2003; Kanaoka et al., 2008). Both of these previous studies imply a potential link between the transcriptional regulation of environmental adaptation and development in plants. O11 physically interacts with ZmICE1 (Figure 11; Supplemental Table 2) and coregulates stress response genes and *ZmYoda* with it (Figure 12), suggesting that O11 and ZmICE1 might coregulate stress responses and endosperm development. We also observed tight correlations between endosperm development and stress responses while investigating *o11*. Plants accumulate abundant free proline under abiotic stress, such as salinity, drought, or extreme temperature (Verbruggen and Hermans, 2008; Szabados and Savouré, 2010). The endosperm of the *o11* mutant contains more than four times the free proline content of the wild type (Supplemental Figure 4B), suggesting that the mutant endosperm is in a state similar to that of abiotic stress. The significant developmental compromise of *o11*, together with the drastic stress response, suggests that O11 might function as a "balancer" between endosperm development and the stress response.

METHODS

Plant Material

The *o11* mutant stock (*o11*-ref) was obtained from the Maize Genetics Cooperation Stock Center (accession number ox-7455). The *o11* mutants were crossed into a W22 genetic background and then self-pollinated to produce F2 populations or backcrossed to the *o11* mutants to produce BC1F1 populations. Kernels from F2 ears were used for cytological and biochemical analyses; the BC1F1 population was used for fine-mapping of *o11*. Root, stem, third leaf, tassel, silk, husk, and ear tissues were collected from five W22 plants at the V12 stage. Immature kernels of W22 plants were harvested at 3, 5, 9, 12, 15, 18, 21, 24, and 27 DAP. All plants were cultivated in a field at the Shanghai University campus in Shanghai, China.

Measurement of Starch, Protein, Lipid, C/N, and Amino Acid Contents

Twenty mature kernels of the wild type or *o11* mutants from the same ears were collected and soaked in water, after which the endosperm was separated from the embryo and pericarp. The wild-type and *o11* mutant endosperm tissues were pooled separately, ground in liquid N_2, and dried to a constant weight for subsequent analysis.

Total starch was measured using an amyloglucosidase/α-amylase starch assay kit (Megazyme) according to the manufacturer's protocol and adapted as follows. A 0.2-mL aliquot of aqueous ethanol (80% [v/v]) was added to a 100-mg sample to aid dispersion, and 3 mL thermostable a-amylase was immediately added. The tube was incubated in a boiling water bath for 6 min and placed in a bath at 50°C; 0.1 mL amyloglucosidase was then added. The tube was stirred with a vortex mixer and incubated at 50°C for 30 min. Duplicate aliquots (0.1 mL) of the diluted solution were transferred to a new tube; 3.0 mL of glucose oxidase/peroxidase (GOPOD) reagent was added, and the tubes were incubated at 50°C for 20 min. The absorbance of each sample and the D-Glc control at 510 nm was measured against the reagent blank.

Total protein, zein and nonzein protein, lipid, total amino acid, and free amino acid contents were measured according to a previously described protocol (Wang et al., 2011). For carbon and nitrogen content measurements, a Vario EL III Element Analyzer was used with the recommended settings.

Each assay above was independently performed three times on the kernels collected from three different ears

Scanning Electron Microscopy and Transmission Electron Microscopy

For scanning electron microscopy, mature wild-type and *o11* kernels harvested from the same self-pollinated ear were analyzed according to a previously described method (Wang et al., 2011). The samples were then observed by scanning electron microscopy (S3400N; Hitachi). For transmission electron microscopy, *o11* and wild-type developing kernels (18 DAP) from the same self-pollinated ear were treated and observed as described previously (Wang et al., 2011). The samples were observed with a Hitachi H7600 transmission electron microscope.

Light Microscopy and Immunofluorescence Assay

For light microscopy analysis, immature wild-type and *o11* mutant kernels at 12, 15, and 18 DAP were collected from the same ear and cut along the

longitudinal axis for paraffin section preparation and along the horizontal axis for resin section preparation. The procedures were performed as described (Chen et al., 2017).

For the immunofluorescence assay, *o11* mutant kernels with no accumulation of O11 protein were used as the negative control. Sections (8 μm thick) of paraffin-embedded samples were rehydrated and blocked with 5% BSA in PBS at pH 7.4 (blocking buffer) and incubated with an O11-specific antibody (dilution of 1:100 in blocking buffer). The samples were then incubated with an anti-rabbit-conjugated fluorescein isothiocyanate antibody (Abcam; ab6717, 1:200) and observed by confocal laser scanning microscopy (LSM710; Zeiss).

Retrotransposon Amplification, Complementation Test, and Allelism Test

The retrotransposon was amplified by DNA polymerase (Toyobo; KOD-401) using a nested PCR strategy. Briefly, PCR was performed with *o11* homozygous mutant genomic DNA using primers retro-1s and retro-1a. Then the first-round PCR product was diluted 100 times and was used as the second-round PCR template (primers were retro-2s and retro-2a) (Supplemental Data Set 9).

For functional complementation tests, genomic DNA (8464 bp) containing the entire coding region, a 2311-bp upstream sequence, and a 1019-bp downstream sequence was amplified from the B73 inbred genome using the primers listed in Supplemental Data Set 9. The fragment was cloned into pTF102 (Frame et al., 2002), and the resulting construct was introduced into *Agrobacterium tumefaciens* strain EHA105 (Frame et al., 2002). Agrobacterium-mediated maize (*Zea mays*) transformation using F2 immature zygotic embryos of the Hi-II hybrid (pApB) was performed according to Frame et al. (2002). Transgenic lines (T0) were hybridized to the homozygous mutant (*o11*/*o11*) and then self-pollinated to harvest O11-functionally complemented ears. F/R6, a marker tightly linked to the *o11* locus, was used to identify homozygous *o11* kernels as PCR products amplified from *o11* homozygous genomic DNA using F/R6 primers were larger than those from pApB genomic DNA.

For the allelism test, a CRISPR-Cas9 vector of *GRMZM2G147685* was constructed as described using a simplex editing strategy (Qi et al., 2016a). The 20-bp target sequence for editing is located in the first exon of *O11* (the 20 bp target sequence is GGGCAACGCCGCCGCGGTGG). Agrobacterium-mediated maize transformation was performed as described above. Five independent Cas9-edited knockout alleles (named *o11-cas9-1* to *o11-cas9-5*) were recovered, and all were separated from the *Cas9* transgene.

Phylogenetic Analysis

Related sequences were identified in the NCBI nr (nonredundant protein sequences) database by performing a BLASTp search with O11 protein sequences. Amino acid sequences were aligned with MUSCLE in the MEGA5.2 software package using the default settings for protein multiple alignment. Evolutionary distances were computed using Poisson correction analysis. The bootstrap method with 1000 replicates for phylogeny testing was used.

Polyclonal Antibody Generation and Immunoblot Analysis

For production of an anti-O11 antibody, the full-length *O11* cDNA was cloned into the *Eco*RI and *Xho*I sites of the pET-32a vector (Novagen) (primers used were 147685-orf-ecori-s and 147685-orf-xhoi-a) and transformed into BL21 cells. For anti-ZmICE1 antibody production, the full-length *ZmIce1* cDNA was cloned into the *Bam*HI and *Xho*I sites of the pET-32a vector (Novagen) (primers used were 173534-orf-bamhi-s and 173534-orf-xhoi-a), which was then transformed into BL21 cells. The recombinant O11- or ICE1-6xHis fusion protein was purified using the ÄKTA purification system with a 1-mL HisTrap FF crude column (GE Healthcare). Both antibodies were prepared in rabbits by Abclonal of China. The primers are listed in Supplemental Data Set 9.

Total protein from wild-type and mutant endosperms was extracted according to the method of Bernard et al. (1994). The protein extracts were quantified by the Bradford assay (Bradford, 1976). Immunoblot analyses were performed as described previously (Wang et al., 2014) using antibodies against the following proteins: O11 (1:1000 dilution), tubulin (Sigma-Aldrich; T6074-200UL; 1:2500 dilution), BiP (Santa Cruz Biotechnology; sc-33757; 1:2000 dilution), H3 (Sigma-Aldrich; H0164-200UL; 1:1000 dilution), and O2 (1:1000 dilution) (Li et al., 2015).

Subcellular Localization of O11 in *Nicotiana benthamiana* and Fractionation of Maize Seed Cytoplasmic and Nuclear Proteins

The open reading frame (ORF) of *O11* was cloned into pENTR/D-TOPO (primers used were O11-topo-s and O11-topo-a listed in Supplemental Data Set 9) using the Gateway TOPO cloning kit (Invitrogen). The right entry clone was introduced into the pB7WGY2 plant expression vector through the LR reaction of the Gateway system (Invitrogen). The expression vectors were transformed into Agrobacterium strain GV3101 as previously described (Wydro et al., 2006). The eYFP signal was observed and imaged using a confocal microscope (LSM710; Zeiss). Fractionation of cytoplasmic and nuclear proteins of 15-DAP maize immature kernels was performed using a previously described method (Qi et al., 2016b).

RNA-Seq and qPCR

Total RNA was extracted from pooled wild-type or *o11* mutant kernels obtained from the same F2 ear at 15 DAP (20 kernels each sample) using Trizol reagent, followed by cleanup and DNase I treatment with the Qiagen RNeasy mini kit in accordance with the protocol provided with the kit. Three independent biological replicates from three different ears were performed. cDNA libraries were constructed following Illumina standard protocols and sequenced with an Illumina HiSeq 2500 by Shanghai Biotechnology. The sequence reads were trimmed using fastx (version: 0.0.13) and mapped to B73 RefGen_v3.24 using TopHat (version: 2.0.9). Cufflinks (version: 2.1.1) was employed to reconstruct the transcripts and to estimate gene expression levels (Trapnell et al., 2010). Significant DEGs were identified as those with a P value of differential expression above the threshold ($P < 0.05$, fold change greater than 1.5). GO enrichment was performed with the accession numbers of significant DEGs via agriGO Singular Enrichment Analysis tool with default parameters (http://bioinfo.cau.edu.cn/agriGO/).

RT-qPCR was performed with SYBR Select Master Mix (Thermo) using a Mastercycler ep realplex 2 (Eppendorf). Levels were calculated using the ΔCt (threshold cycle) method and the maize *Actin* gene was used as the reference. All primers used in the study are listed in Supplemental Data Set 9.

ChIP-Seq and ChIP-qPCR

For ChIP-Seq, ChIP using an antibody against O11 with pooled W22 or *o11* mutant kernels at 15 DAP was performed as previously described (Kaufmann et al., 2010; Li et al., 2015). Two independent biological replicates prepared at different times were performed. Briefly, dissected 15 DAP kernels were immediately cross-linked in buffer containing 1% formaldehyde on ice under vacuum for 15 min, after which the vacuum was released and reapplied for another 14 min. Fixation was stopped by adding 1.25 M glycine. The cross-linked kernels were dried and ground into powder in liquid N_2, followed by nuclear isolation and sonication. Protein A-agarose beads (Millipore) and an antibody against O11 were used to precipitate the DNA, which was digested by proteinase K, recovered using a QIAquick PCR purification kit (Qiagen) and analyzed by qPCR (Supplemental Data Set 9). ChIP-DNA libraries were constructed and

sequenced by Shanghai Hanyu Bio-Tech. Briefly, DNA samples were end-repaired, followed by A-base addition and ligation with adapters using TruSeq PE Cluster Kit (Illumina). After PCR enrichment, the DNA library was quantified with Qubit (Thermo Fisher), followed by cBot cluster generation (Illumina) and library sequencing with an Illumina HiSeq 2500.

ChIP was performed using the same protocol as for ChIP-seq. For ChIP-qPCR of ZmICE1, a ZmICE1-specific antibody was used to precipitate the chromatin; IgG was used as an antibody control. In brief, the level of each gene in three biological replicates was normalized to that of *Actin* measured in the sample with SYBR Select Master Mix (Thermo) using a Mastercycler ep realplex 2 (Eppendorf). Levels were calculated using the ΔCt (threshold cycle) method. The primers used for ChIP-qPCR are listed in Supplemental Data Set 9.

ChIP-Seq Data Analysis

Raw fastq data were trimmed using the SolexaQA++ v2.5 program with Q20 (Phred score >20) and L40 (length >40). The cleaned reads were then aligned to the maize B73 reference genome (AGPv3; http://plants.ensembl.org/) using Bowtie2 (v2.3.2) with default parameters (Langmead et al., 2009). Unique aligned reads were extracted by the SAMtools v1.2 program with ~~a~~ MAQ20 (map quality >20) filtration. Peak calling was performed separately for each biological replicate using MACS2 (v2.1.0) (bandwidth = 300; model fold = [10, 30]; q-value cutoff = 0.01) (Zhang et al., 2008). Significant peaks with high confidence in both biological replicates were considered to be consistent peaks. To search for conserved binding motifs in consistent O11 binding regions, the 500-bp sequence surrounding the peak summit of each consistent peak was extracted and submitted to the online version of MEME-ChIP (Machanick and Bailey, 2011) under default settings. A custom background model derived from JASPAR CORE (2016) plants was provided, and "any number of repetitions" of a motif was allowed.

GC-MS

Metabolite analysis by GC-MS was performed according to a described method, with the following minor modifications (Fait et al., 2006). Briefly, 250 mg maize endosperm was homogenized in liquid N_2 and extracted with methanol:chloroform:water extraction solution (900 μL, 1:2.5:1 v/v). A standard (0.2 mg mL^{-1} ribitol in water) was added as for quantification. The mixture was extracted for 15 min at 4°C with shaking. After centrifugation at 2200*g* for 2 min, 400 μL water was added to the supernatant. Following vortexing and centrifugation, the methanol-water phase was collected, and 300 μL was reduced to dryness under vacuum. The residue was redissolved and derivatized for 90 min at 37°C (in 60 μL 20 mg mL^{-1} methoxyamine hydrochloride in pyridine) followed by a 30-min treatment with 90 μL *N*-methyl-*N*-(trimethylsilyl)trifluoroacetamide at 37°C. GC-MS analysis was performed using an Agilent 6890 gas chromatograph coupled to a 5975C inert MS detector (Agilent Technologies) equipped with a capillary column (HP-5MS) with an internal diameter of 250 μm, a length of 30 m, and a film thickness of 0.25 μm. Helium was used as the carrier gas at a flow rate of 1 mL/min. The injection volume was 5 μL. Splitless injection mode was used for all samples. The optimized GC-MS front inlet temperature was 220°C. Oven temperature was set at an initial temperature of 60°C, held for 2 min, increased to 180°C at 5°C/min, and then increased to 260°C at 10°C/min, where it was held for 5 min. The instrument was operated using an electron ionization source at 70 eV, and the MS source and quad temperatures were 230°C and 150°C, respectively. The scanning range was 40 to 700 (mass-to-charge ratio). Products were identified by comparison with standards and the NIST (National Institute of Standards and Technology) library. Peak areas of wild-type and *o11* metabolites were normalized by the internal standard ribitol, which was derivatized concomitantly with the tissue samples, and were compared with the mean peak area calculated from the corresponding wild type. Three biological replicates were produced from three independently pooled wild-type or *o11* endosperm. For peak area of the carbohydrate metabolites, see Supplemental Table 1.

Y2H Assay and Yeast Transactivation Assay

The full-length ORF of *O11* was fused to the GAL4 BD domain in pGBKT7 at the *Nco*I and *Eco*RI sites using primers O11-ncoI-orf-s and O11-ecori-orf-a (Supplemental Data Set 9). We used this bait to screen a maize developing kernel cDNA library fused downstream of the GAL4 AD domain in pGADT7 (Wang et al., 2010). The *O2* ORF was fused to pGADT7 at the *Xma*I and *Cla*I sites. The yeast transactivation assay was performed as previously described (Qiao et al., 2016). The full-length *O11* cDNA was cloned into the pGBK-T7 vector and co-transformed into the EGY48 yeast strain with the pG221 vector. The pG221 vector contains a minimal promoter that is bound by the DNA binding motif encoded by the pGBK-T7 vector. The empty pGBK-T7 vector was used as a negative control. pGBK-T7-O2 containing the full-length *O2* ORF was used as a positive control.

Transient Transcription Dual-LUC Assay

Dual-LUC assays using *N. benthamiana* plants were performed as described previously (Hellens et al., 2005; Liu et al., 2008). The luciferase activity of the plant extract was analyzed by a luminometer (Promega 20/20) using commercial LUC reaction reagents according to the manufacturer's instructions (Promega). For dual-LUC assays, three independent experiments at different times (biological triplicates) were performed.

For the effectors used in this study, the full-length ORF of *O11* or ZmICE1 was fused into the overexpression vector (pHB) (Yao et al., 2016) using primers O11-hindiii-ORF-S and O11-saci-ORF-A, or 173534-orf-bamhi-s and 173534-ORF-xbai-A, respectively. For the reporters, the promoters of O11-potential targets (about −1 kb to 0 bp of start codon) were cloned into pGreenII0800-LUC (the specific restriction enzyme sites and primers used are indicated in Supplemental Data Set 9).

LCI Assay

The ORFs of *O11* and *O2* and the 18 potential genes encoding O11-interacting proteins identified from Y2H screening were cloned into both JW771 (NLUC) and JW772 (CLUC) (Zhang et al., 2015) using ClonExpress II One Step Cloning Kit (Vazyme) (the primers are listed in Supplemental Data Set 9). The constructs were transformed into Agrobacterium strain GV3101. The Agrobacterium (strain GV3101) cells were grown to OD_{600} = 0.8, pelleted, and resuspended in infiltration buffer (10 mM methylester sulfonate, 10 mM $MgCl_2$, and 150 μM acetosyringone, pH 5.7) and infiltrated into 3-week-old *N. benthamiana* leaves using a needleless syringe in the different combinations indicated in Figure 11. After 48 h under the condition of 16 h of light and 8 h of dark, leaves were injected with 1 mM luciferin (Promega). The resulting luciferase signals were collected using the Tanon-5200 image system. The LCI assay was performed three times independently.

Accession Numbers

Sequence data from this article can be found in the GenBank/EMBL data libraries under the following accession numbers: O11, DAA37785.1, *GRMZM2G147685*; ZmICE1, NP_001131774.2, *GRMZM2G173534*; ZmYODA, NP_001308276.1, *GRMZM2G093316*; O2, XP_008651859.1, *GRMZM2G015534*; PBF, NP_001105400.2, *GRMZM2G146283*; cyPPDK1, AFW77961.1, *GRMZM2G306345*; cyPPDK2, XP_008656296.1, *GRMZM2G097457*; NKD2, NP_001159309.1, *GRMZM5G884137*; ZmDOF3, NP_001131758.1C, *GRMZM2G137502*; AtZOU, NP_175399.2, *AT1G49770*; AtICE1, NP_189309.2, *AT3G26744*; AtYODA, and NP_176557.1, *AT1G63700*. Sequences used for phylogenetic analysis are as follows: *Sorghum bicolor*, KXG26314.1;

Setaria italica, KQK97270.1; *Oryza sativa japonica* group, XP_015635110.1; *Brachypodium distachyon*, XM_003572553.1; *Aegilops tauschii*, KD581806.1; *Hordeum vulgare* subsp *Vulgare*, dbj|AK373155.1; *Arabidopsis thaliana* (AtZOU), OAP16519.1; *Brassica napus*, XP_013752539.1. *Populus euphratica*, XP_011000121.1; *Vitis vinifera*, XP_002282369.1; *Solanum tuberosum*, XP_015163703.1; *Nicotiana tabacum*, XP_016454613.1; *Gossypium raimondii*, XP_012466617.1; *Manihot esculenta*, OAY50956.1; *Ricinus communis*, EEF52378.1; and *Physcomitrella patens*, XP_001778019.1. RNA-seq and ChIP-seq data are available from National Center for Biotechnology Information Gene Expression Omnibus (http://www.ncbi.nlm.nih.gov/geo) under the series entries GSE97422 and GSE102051.

Supplemental Data

Supplemental Figure 1. Phenotype and dry weight analysis from kernels of *o11*xW22 F2 ears.

Supplemental Figure 2. Paraffin sections of 18 DAP wild-type and *o11* kernels for full-kernel images.

Supplemental Figure 3. Comparison of starch, protein (total protein, zein, and nonzein), and lipid accumulation in the mature wild-type and *o11* endosperm according to weight.

Supplemental Figure 4. Analysis of total amino acid and free amino acid contents of the wild type and *o11* mature endosperm.

Supplemental Figure 5. *GRMZM2G147685* knockout alleles and allelism test with *o11.*

Supplemental Figure 6. Diagram showing the O11 protein sequence and its homologs in monocotyledonous species (*Sorghum bicolor*, *Setaria italica*, and *Oryza sativa japonica* group) and dicotyledonous species (*Arabidopsis thaliana* and *Brassica napus*).

Supplemental Figure 7. Determination of anti-O11 antibody specificity.

Supplemental Figure 8. EMSA assay and transient transcription dual-luciferase (dual-LUC) assays using the promoters of O11 target genes with the wild type (Gwt) and mutant version (Gmu) of the G-box (CACGTG).

Supplemental Figure 9. GO classification of genes with promoter regions that are directly bound by O11, as identified by ChIP-seq.

Supplemental Figure 10. O11 does not interact with O2 in a yeast two-hybrid assay or an LCI assay.

Supplemental Figure 11. Determination of the ZmICE1 antibody specificity.

Supplemental Figure 12. Full scan images of immunoblots.

Supplemental Table 1. Peak area of the carbohydrate metabolites of wild type and *o11* endosperm.

Supplemental Table 2. List of O11-interacting proteins, as identified by a Y2H assay.

Supplemental Table 3. Normalized expression levels in FPKM for *O11*, *ZmIce1*, and *ZmYoda* in different compartments of the maize kernel from LCM RNA-seq data (Zhan et al., 2015).

Supplemental Data Set 1. Text file of the alignment used for the phylogenetic analysis shown in Figure 5A.

Supplemental Data Set 2. Significantly differentially expressed genes identified from RNA-seq data for *o11* at 15 DAP.

Supplemental Data Set 3. Gene Ontology classifications of *o11* DEGs with functional annotations.

Supplemental Data Set 4. O11 binding sites identified by ChIP-Seq.

Supplemental Data Set 5. Gene Ontology classifications of O11 ChIP binding sites (promoter region) with functional annotations.

Supplemental Data Set 6. The 259 high-confidence potential targets of O11.

Supplemental Data Set 7. Overlapping peaks between O11 and O2 across the genome.

Supplemental Data Set 8. Genes bound by both O11 and O2 in 15-DAP developing endosperm.

Supplemental Data Set 9. List of primers.

Supplemental File 1. Student's *t* test tables.

ACKNOWLEDGMENTS

We thank Lin Xu (Shanghai Institute of Plant Physiology and Ecology, SIBS) for technical support with ChIP experiments. We thank Yanan Feng and Huiling Ling for technical support with Y2H and maize transformation experiments. This work was supported by the National Natural Sciences Foundation of China (91635303), the National Key Research and Development Program of China (2016YFD0101003), and the National Natural Science Foundation of China (31425019, 91335208, and 31401386).

AUTHOR CONTRIBUTIONS

R.S., F.F., and W.Q. designed the research. F.F., S.Y., L.X., W.Y., and Y.C. performed the experiments. F.F., R.S., W.Q., Y.L., and H.Z. analyzed the data. F.F., R.S., and W.Q. wrote the article.

Received August 2, 2017; revised January 22, 2018; accepted February 6, 2018; published February 7, 2018.

REFERENCES

Ambrose, B.A., Lerner, D.R., Ciceri, P., Padilla, C.M., Yanofsky, M.F., and Schmidt, R.J. (2000). Molecular and genetic analyses of the silky1 gene reveal conservation in floral organ specification between eudicots and monocots. Mol. Cell **5:** 569–579.

Becraft, P.W., and Gutierrez-Marcos, J. (2012). Endosperm development: dynamic processes and cellular innovations underlying sibling altruism. Wiley Interdiscip. Rev. Dev. Biol. **1:** 579–593.

Bergmann, D.C., Lukowitz, W., and Somerville, C.R. (2004). Stomatal development and pattern controlled by a MAPKK kinase. Science **304:** 1494–1497.

Bernard, L., Ciceri, P., and Viotti, A. (1994). Molecular analysis of wild-type and mutant alleles at the Opaque-2 regulatory locus of maize reveals different mutations and types of O2 products. Plant Mol. Biol. **24:** 949–959.

Bradford, M.M. (1976). A rapid and sensitive method for the quantitation of microgram quantities of protein utilizing the principle of protein-dye binding. Anal. Biochem. **72:** 248–254.

Breuninger, H., Rikirsch, E., Hermann, M., Ueda, M., and Laux, T. (2008). Differential expression of WOX genes mediates apical-basal axis formation in the Arabidopsis embryo. Dev. Cell **14:** 867–876.

Chen, X., Feng, F., Qi, W., Xu, L., Yao, D., Wang, Q., and Song, R. (2017). Dek35 encodes a PPR protein that affects cis-splicing of mitochondrial nad4 intron 1 and seed development in maize. Mol. Plant **10:** 427–441.

Chinnusamy, V., Ohta, M., Kanrar, S., Lee, B.H., Hong, X., Agarwal, M., and Zhu, J.K. (2003). ICE1: a regulator of cold-induced transcriptome and freezing tolerance in Arabidopsis. Genes Dev. **17:** 1043–1054.

Cifuentes-Esquivel, N., Bou-Torrent, J., Galstyan, A., Gallemí, M., Sessa, G., Salla Martret, M., Roig-Villanova, I., Ruberti, I., and Martínez-García, J.F. (2013). The bHLH proteins BEE and BIM positively modulate the shade avoidance syndrome in Arabidopsis seedlings. Plant J. **75:** 989–1002.

Denay, G., Creff, A., Moussu, S., Wagnon, P., Thévenin, J., Gérentes, M.F., Chambrier, P., Dubreucq, B., and Ingram, G. (2014). Endosperm breakdown in Arabidopsis requires heterodimers of the basic helix-loop-helix proteins ZHOUPI and INDUCER OF CBP EXPRESSION 1. Development **141:** 1222–1227.

Dickinson, D.B., and Preiss, J. (1969). Presence of ADP-glucose pyrophosphorylase in Shrunken-2 and Brittle-2 mutants of maize endosperm. Plant Physiol. **44:** 1058–1062.

Fait, A., Angelovici, R., Less, H., Ohad, I., Urbanczyk-Wochniak, E., Fernie, A.R., and Galili, G. (2006). Arabidopsis seed development and germination is associated with temporally distinct metabolic switches. Plant Physiol. **142:** 839–854.

Fourquin, C., Beauzamy, L., Chamot, S., Creff, A., Goodrich, J., Boudaoud, A., and Ingram, G. (2016). Mechanical stress mediated by both endosperm softening and embryo growth underlies endosperm elimination in Arabidopsis seeds. Development **143:** 3300–3305.

Frame, B.R., Shou, H., Chikwamba, R.K., Zhang, Z., Xiang, C., Fonger, T.M., Pegg, S.E., Li, B., Nettleton, D.S., Pei, D., and Wang, K. (2002). Agrobacterium tumefaciens-mediated transformation of maize embryos using a standard binary vector system. Plant Physiol. **129:** 13–22.

Gontarek, B.C., Neelakandan, A.K., Wu, H., and Becraft, P.W. (2016). NKD transcription factors are central regulators of maize endosperm development. Plant Cell **28:** 2916–2936.

Gregis, V., et al. (2013). Identification of pathways directly regulated by SHORT VEGETATIVE PHASE during vegetative and reproductive development in Arabidopsis. Genome Biol. **14:** R56.

Grimault, A., Gendrot, G., Chamot, S., Widiez, T., Rabillé, H., Gérentes, M.F., Creff, A., Thévenin, J., Dubreucq, B., Ingram, G.C., Rogowsky, P.M., and Depège-Fargeix, N. (2015). ZmZHOUPI, an endosperm-specific basic helix-loop-helix transcription factor involved in maize seed development. Plant J. **84:** 574–586.

Hartmann, U., Höhmann, S., Nettesheim, K., Wisman, E., Saedler, H., and Huijser, P. (2000). Molecular cloning of SVP: a negative regulator of the floral transition in Arabidopsis. Plant J. **21:** 351–360.

Hellens, R.P., Allan, A.C., Friel, E.N., Bolitho, K., Grafton, K., Templeton, M.D., Karunairetnam, S., Gleave, A.P., and Laing, W.A. (2005). Transient expression vectors for functional genomics, quantification of promoter activity and RNA silencing in plants. Plant Methods **1:** 13.

Hoecker, U., Vasil, I.K., and McCarty, D.R. (1995). Integrated control of seed maturation and germination programs by activator and repressor functions of Viviparous-1 of maize. Genes Dev. **9:** 2459–2469.

Hu, Y., Jiang, L., Wang, F., and Yu, D. (2013). Jasmonate regulates the inducer of cbf expression-C-repeat binding factor/DRE binding factor1 cascade and freezing tolerance in Arabidopsis. Plant Cell **25:** 2907–2924.

James, M.G., Denyer, K., and Myers, A.M. (2003). Starch synthesis in the cereal endosperm. Curr. Opin. Plant Biol. **6:** 215–222.

Kanaoka, M.M., Pillitteri, L.J., Fujii, H., Yoshida, Y., Bogenschutz, N.L., Takabayashi, J., Zhu, J.K., and Torii, K.U. (2008). SCREAM/ICE1 and SCREAM2 specify three cell-state transitional steps leading to arabidopsis stomatal differentiation. Plant Cell **20:** 1775–1785.

Kaufmann, K., Muiño, J.M., Østerås, M., Farinelli, L., Krajewski, P., and Angenent, G.C. (2010). Chromatin immunoprecipitation (ChIP) of plant transcription factors followed by sequencing (ChIP-SEQ) or hybridization to whole genome arrays (ChIP-CHIP). Nat. Protoc. **5:** 457–472.

Kiesselbach, T.A. (1949). The structure and reproduction of corn. Nebr. Agric. Exp. Stn. Res. Bull. **161:** 1–96.

Kim, T.W., Michniewicz, M., Bergmann, D.C., and Wang, Z.Y. (2012). Brassinosteroid regulates stomatal development by GSK3-mediated inhibition of a MAPK pathway. Nature **482:** 419–422.

Klimczak, L.J., Schindler, U., and Cashmore, A.R. (1992). DNA binding activity of the Arabidopsis G-box binding factor GBF1 is stimulated by phosphorylation by casein kinase II from broccoli. Plant Cell **4:** 87–98.

Krogan, N.T., and Long, J.A. (2009). Why so repressed? Turning off transcription during plant growth and development. Curr. Opin. Plant Biol. **12:** 628–636.

Leroux, B.M., Goodyke, A.J., Schumacher, K.I., Abbott, C.P., Clore, A.M., Yadegari, R., Larkins, B.A., and Dannenhoffer, J.M. (2014). Maize early endosperm growth and development: from fertilization through cell type differentiation. Am. J. Bot. **101:** 1259–1274.

Langmead, B., Trapnell, C., Pop, M., and Salzberg, S.L. (2009). Ultrafast and memory-efficient alignment of short DNA sequences to the human genome. Genome Biol. **10:** R25.

Li, C., Qiao, Z., Qi, W., Wang, Q., Yuan, Y., Yang, X., Tang, Y., Mei, B., Lv, Y., Zhao, H., Xiao, H., and Song, R. (2015). Genome-wide characterization of cis-acting DNA targets reveals the transcriptional regulatory framework of opaque2 in maize. Plant Cell **27:** 532–545.

Lie, C., Kelsom, C., and Wu, X. (2012). WOX2 and STIMPY-LIKE/WOX8 promote cotyledon boundary formation in Arabidopsis. Plant J. **72:** 674–682.

Liu, H., Yu, X., Li, K., Klejnot, J., Yang, H., Lisiero, D., and Lin, C. (2008). Photoexcited CRY2 interacts with CIB1 to regulate transcription and floral initiation in Arabidopsis. Science **322:** 1535–1539.

Lukowitz, W., Roeder, A., Parmenter, D., and Somerville, C. (2004). A MAPKK kinase gene regulates extra-embryonic cell fate in Arabidopsis. Cell **116:** 109–119.

Machanick, P., and Bailey, T.L. (2011). MEME-ChIP: motif analysis of large DNA datasets. Bioinformatics **27:** 1696–1697.

Manicacci, D., et al. (2009). Epistatic interactions between Opaque2 transcriptional activator and its target gene CyPPDK1 control kernel trait variation in maize. Plant Physiol. **150:** 506–520.

Miclaus, M., Wu, Y., Xu, J.H., Dooner, H.K., and Messing, J. (2011). The maize high-lysine mutant opaque7 is defective in an acyl-CoA synthetase-like protein. Genetics **189:** 1271–1280.

McCarty, D.R., Hattori, T., Carson, C.B., Vasil, V., Lazar, M., and Vasil, I.K. (1991). The Viviparous-1 developmental gene of maize encodes a novel transcriptional activator. Cell **66:** 895–905.

Myers, A.M., James, M.G., Lin, Q., Yi, G., Stinard, P.S., Hennen-Bierwagen, T.A., and Becraft, P.W. (2011). Maize opaque5 encodes monogalactosyldiacylglycerol synthase and specifically affects galactolipids necessary for amyloplast and chloroplast function. Plant Cell **23:** 2331–2347.

Nelson, O. (1981). The mutations opaque-9 through opaque-13. Corn Genet. Coop Newslett. **55:** 68.

Oh, E., Zhu, J.Y., and Wang, Z.Y. (2012). Interaction between BZR1 and PIF4 integrates brassinosteroid and environmental responses. Nat. Cell Biol. **14:** 802–809.

Oh, E., Kang, H., Yamaguchi, S., Park, J., Lee, D., Kamiya, Y., and Choi, G. (2009). Genome-wide analysis of genes targeted by PHYTOCHROME INTERACTING FACTOR 3-LIKE5 during seed germination in Arabidopsis. Plant Cell **21:** 403–419.

Ohashi-Ito, K., and Bergmann, D.C. (2007). Regulation of the Arabidopsis root vascular initial population by LONESOME HIGHWAY. Development **134:** 2959–2968.

Olsen, O.A. (2001). Endosperm development: cellularization and cell fate specification. Annu. Rev. Plant Physiol. Plant Mol. Biol. **52:** 233–267.

Olsen, O.A. (2004). Nuclear endosperm development in cereals and *Arabidopsis thaliana*. Plant Cell **16** (suppl.): S214–S227.

Opsahl-Ferstad, H.G., Le Deunff, E., Dumas, C., and Rogowsky, P.M. (1997). ZmEsr, a novel endosperm-specific gene expressed in a restricted region around the maize embryo. Plant J. **12:** 235–246.

Preiss, J., Danner, S., Summers, P.S., Morell, M., Barton, C.R., Yang, L., and Nieder, M. (1990). Molecular characterization of the Brittle-2 gene effect on maize endosperm ADPglucose pyrophosphorylase subunits. Plant Physiol. **92:** 881–885.

Prioul, J.L., Méchin, V., and Damerval, C. (2008). Molecular and biochemical mechanisms in maize endosperm development: the role of pyruvate-Pi-dikinase and Opaque-2 in the control of C/N ratio. C. R. Biol. **331:** 772–779.

Qi, W., Zhu, T., Tian, Z., Li, C., Zhang, W., and Song, R. (2016a). High-efficiency CRISPR/Cas9 multiplex gene editing using the glycine tRNA-processing system-based strategy in maize. BMC Biotechnol. **16:** 58.

Qi, W., Zhu, J., Wu, Q., Wang, Q., Li, X., Yao, D., Jin, Y., Wang, G., Wang, G., and Song, R. (2016b). Maize reas1 mutant stimulates ribosome use efficiency and triggers distinct transcriptional and translational responses. Plant Physiol. **170:** 971–988.

Qi, X., Li, S., Zhu, Y., Zhao, Q., Zhu, D., and Yu, J. (2017). ZmDof3, a maize endosperm-specific Dof protein gene, regulates starch accumulation and aleurone development in maize endosperm. Plant Mol. Biol. **93:** 7–20.

Qiao, Z., Qi, W., Wang, Q., Feng, Y., Yang, Q., Zhang, N., Wang, S., Tang, Y., and Song, R. (2016). ZmMADS47 regulates zein gene transcription through interaction with Opaque2. PLoS Genet. **12:** e1005991.

Qu, J., Ma, C., Feng, J., Xu, S., Wang, L., Li, F., Li, Y., Zhang, R., Zhang, X., Xue, J., and Guo, D. (2016). Transcriptome dynamics during maize endosperm development. PLoS One **11:** e0163814.

Russell, S.D. (1992). Double fertilization. Int. Rev. Cytol. **140:** 357–388.

Schmidt, R.J., Burr, F.A., and Burr, B. (1987). Transposon tagging and molecular analysis of the maize regulatory locus opaque-2. Science **238:** 960–963.

Schönrock, N., Bouveret, R., Leroy, O., Borghi, L., Köhler, C., Gruissem, W., and Hennig, L. (2006). Polycomb-group proteins repress the floral activator AGL19 in the FLC-independent vernalization pathway. Genes Dev. **20:** 1667–1678.

Seo, P.J., Park, J.M., Kang, S.K., Kim, S.G., and Park, C.M. (2011). An Arabidopsis senescence-associated protein SAG29 regulates cell viability under high salinity. Planta **233:** 189–200.

Sheen, J. (1991). Molecular mechanisms underlying the differential expression of maize pyruvate, orthophosphate dikinase genes. Plant Cell **3:** 225–245.

Szabados, L., and Savouré, A. (2010). Proline: a multifunctional amino acid. Trends Plant Sci. **15:** 89–97.

Trapnell, C., Williams, B.A., Pertea, G., Mortazavi, A., Kwan, G., van Baren, M.J., Salzberg, S.L., Wold, B.J., and Pachter, L. (2010). Transcript assembly and quantification by RNA-seq reveals unannotated transcripts and isoform switching during cell differentiation. Nat. Biotechnol. **28:** 511–515.

Verbruggen, N., and Hermans, C. (2008). Proline accumulation in plants: a review. Amino Acids **35:** 753–759.

Vicente-Carbajosa, J., Moose, S.P., Parsons, R.L., and Schmidt, R.J. (1997). A maize zinc-finger protein binds the prolamin box in zein gene promoters and interacts with the basic leucine zipper transcriptional activator Opaque2. Proc. Natl. Acad. Sci. USA **94:** 7685–7690.

Wang, G., Sun, X., Wang, G., Wang, F., Gao, Q., Sun, X., Tang, Y., Chang, C., Lai, J., Zhu, L., Xu, Z., and Song, R. (2011). Opaque7 encodes an acyl-activating enzyme-like protein that affects storage protein synthesis in maize endosperm. Genetics **189:** 1281–1295.

Wang, G., Wang, F., Wang, G., Wang, F., Zhang, X., Zhong, M., Zhang, J., Lin, D., Tang, Y., Xu, Z., and Song, R. (2012). Opaque1 encodes a myosin XI motor protein that is required for endoplasmic reticulum motility and protein body formation in maize endosperm. Plant Cell **24:** 3447–3462.

Wang, G., Wang, H., Zhu, J., Zhang, J., Zhang, X., Wang, F., Tang, Y., Mei, B., Xu, Z., and Song, R. (2010). An expression analysis of 57 transcription factors derived from ESTs of developing seeds in Maize (*Zea mays*). Plant Cell Rep. **29:** 545–559.

Wang, G., Zhang, J., Wang, G., Fan, X., Sun, X., Qin, H., Xu, N., Zhong, M., Qiao, Z., Tang, Y., and Song, R. (2014). Proline responding1 plays a critical role in regulating general protein synthesis and the cell cycle in maize. Plant Cell **26:** 2582–2600.

Wang, H., Ngwenyama, N., Liu, Y., Walker, J.C., and Zhang, S. (2007). Stomatal development and patterning are regulated by environmentally responsive mitogen-activated protein kinases in Arabidopsis. Plant Cell **19:** 63–73.

Wu, X., Chory, J., and Weigel, D. (2007). Combinations of WOX activities regulate tissue proliferation during Arabidopsis embryonic development. Dev. Biol. **309:** 306–316.

Wu, Y., and Messing, J. (2012). Rapid divergence of prolamin gene promoters of maize after gene amplification and dispersal. Genetics **192:** 507–519.

Wu, Y., and Messing, J. (2010). RNA interference-mediated change in protein body morphology and seed opacity through loss of different zein proteins. Plant Physiol. **153:** 337–347.

Wydro, M., Kozubek, E., and Lehmann, P. (2006). Optimization of transient Agrobacterium-mediated gene expression system in leaves of *Nicotiana benthamiana*. Acta Biochim. Pol. **53:** 289–298.

Xing, Q., Creff, A., Waters, A., Tanaka, H., Goodrich, J., and Ingram, G.C. (2013). ZHOUPI controls embryonic cuticle formation via a signalling pathway involving the subtilisin protease ABNORMAL LEAF-SHAPE1 and the receptor kinases GASSHO1 and GASSHO2. Development **140:** 770–779.

Xu, X., Chen, C., Fan, B., and Chen, Z. (2006). Physical and functional interactions between pathogen-induced Arabidopsis WRKY18, WRKY40, and WRKY60 transcription factors. Plant Cell **18:** 1310–1326.

Yang, S., Johnston, N., Talideh, E., Mitchell, S., Jeffree, C., Goodrich, J., and Ingram, G. (2008). The endosperm-specific ZHOUPI gene of Arabidopsis thaliana regulates endosperm breakdown and embryonic epidermal development. Development **135:** 3501–3509.

Yao, D., Qi, W., Li, X., Yang, Q., Yan, S., Ling, H., Wang, G., Wang, G., and Song, R. (2016). Maize opaque10 encodes a cereal-specific protein that is essential for the proper distribution of zeins in endosperm protein bodies. PLoS Genet. **12:** e1006270.

Yi, G., Neelakandan, A.K., Gontarek, B.C., Vollbrecht, E., and Becraft, P.W. (2015). The naked endosperm genes encode duplicate INDETERMINATE domain transcription factors required for maize endosperm cell patterning and differentiation. Plant Physiol. **167:** 443–456.

Zhan, J., Thakare, D., Ma, C., Lloyd, A., Nixon, N.M., Arakaki, A.M., Burnett, W.J., Logan, K.O., Wang, D., Wang, X., Drews, G.N., and Yadegari, R. (2015). RNA sequencing of laser-capture microdissected

compartments of the maize kernel identifies regulatory modules associated with endosperm cell differentiation. Plant Cell **27:** 513–531.

Zhang, Y., Liu, T., Meyer, C.A., Eeckhoute, J., Johnson, D.S., Bernstein, B.E., Nusbaum, C., Myers, R.M., Brown, M., Li, W., and Liu, X.S. (2008). Model-based analysis of ChIP-Seq (MACS). Genome Biol. **9:** R137.

Zhang, Y., Mayba, O., Pfeiffer, A., Shi, H., Tepperman, J.M., Speed, T.P., and Quail, P.H. (2013). A quartet of PIF bHLH factors provides a transcriptionally centered signaling hub that regulates seedling morphogenesis through differential expression-patterning of shared target genes in Arabidopsis. PLoS Genet. **9:** e1003244.

Zhang, Z., Yang, J., and Wu, Y. (2015). Transcriptional regulation of zein gene expression in maize through the additive and synergistic action of opaque2, prolamine-box binding factor, and O2 heterodimerizing proteins. Plant Cell **27:** 1162–1172.

Zhang, Z., Zheng, X., Yang, J., Messing, J., and Wu, Y. (2016). Maize endosperm-specific transcription factors O2 and PBF network the regulation of protein and starch synthesis. Proc. Natl. Acad. Sci. USA **113:** 10842–10847.